CARDIFF UNIVERSITY
PRIFYSGOL CAERDYDD

ORCA – Online Research @ Cardiff

This is an Open Access document downloaded from ORCA, Cardiff University's institutional repository:https://orca.cardiff.ac.uk/id/eprint/110828/

This is the author's version of a work that was submitted to / accepted for publication.

Citation for final published version:

Nelson, Nya D., Dodson, Lois M., Escudero-Monreal, Laura, Sukumar, Ann T., Williams, Christopher L., Mihalek, Ivana, Baldan, Alessandro, Baird, Duncan M. and Bertuch, Alison A. 2018. The C-terminal extension unique to the long isoform of the shelterin component TIN2 enhances its interaction with TRF2 in a phosphorylation- and dyskeratosis congenita-cluster-dependent fashion. Molecular and Cellular Biology 38 (12) , e00025-18. 10.1128/MCB.00025-18

Publishers page: http://dx.doi.org/10.1128/MCB.00025-18

Please note:
Changes made as a result of publishing processes such as copy-editing, formatting and page numbers may not be reflected in this version. For the definitive version of this publication, please refer to the published source. You are advised to consult the publisher's version if you wish to cite this paper.

This version is being made available in accordance with publisher policies. See http://orca.cf.ac.uk/policies.html for usage policies. Copyright and moral rights for publications made available in ORCA are retained by the copyright holders.

1 The C-terminal extension unique to the long isoform of the shelterin component TIN2
2 enhances its interaction with TRF2 in a phosphorylation- and dyskeratosis congenita-
3 cluster-dependent fashion

4 Running title: Differential interactions of TIN2 isoforms

5 Nya D. Nelson[1,2], Lois M. Dodson[1,2], Laura Escudero[3], Ann T. Sukumar[1], Christopher L.
6 Williams[2], Ivana Mihalek[4], Alessandro Baldan[1,2], Duncan M. Baird[3], and Alison A.
7 Bertuch#[1,2]

8 [1]Department of Molecular & Human Genetics, Baylor College of Medicine, Houston, TX

9 [2]Division of Hematology/Oncology, Department of Pediatrics, Baylor College of
10 Medicine, Houston, TX

11 [3]Division of Cancer and Genetics, School of Medicine, Cardiff University, Cardiff, UK

12 [4]Bioinformatics Institute, Agency for Science Technology and Research, Singapore

13 # Corresponding author email: abertuch@bcm.edu

14

15 Present affiliations:

16 Nya Nelson: Department of Pathology and Laboratory Medicine, Hospital of the
17 University of Pennsylvania, Philadelphia, PA

18 Laura Escudero: Translational Research Program, Vall d'Hebron Institute of Oncology,
19 Barcelona, Spain.

20

21 Word count for Materials and Methods: 2,161

22 Word count for Introduction, Results, and Discussion: 5,480

23 **ABSTRACT**

24 TIN2 is central to the shelterin complex, linking the telomeric proteins TRF1 and
25 TRF2 with TPP1/POT1. Mutations in *TINF2*, which encodes TIN2, that are found in
26 dyskeratosis congenita (DC) result in very short telomeres and cluster in a region
27 shared by the two TIN2 isoforms, TIN2S (short) and TIN2L (long). Here we show that
28 TIN2L, but not TIN2S, is phosphorylated. TRF2 interacts more with TIN2L than TIN2S,
29 and both the DC-cluster and phosphorylation promote this enhanced interaction. The
30 binding of TIN2L, but not TIN2S, is affected by TRF2-F120, which is also required for
31 TRF2's interaction with end processing factors such as Apollo. Conversely, TRF1
32 interacts more with TIN2S than with TIN2L. A DC-associated mutation further reduces
33 TIN2L-TRF1, but not TIN2S-TRF1, interaction. Cells overexpressing TIN2L or
34 phosphomimetic-TIN2L are permissive to telomere elongation, whereas cells
35 overexpressing TIN2S or phosphodead-TIN2L are not. Telomere lengths are
36 unchanged in cell lines in which TIN2L expression has been eliminated by
37 CRISPR/Cas9-mediated mutation. These results indicate that TIN2 isoforms are
38 biochemically and functionally distinguishable, and that shelterin composition could be
39 fundamentally altered in patients with *TINF2* mutations.

40

INTRODUCTION

The stability of the natural ends of linear chromosomes can be compromised by two major processes: progressive shortening with each round of DNA replication, due to the so-called end-replication problem, and misrecognition of the ends as DNA double strand breaks (DSBs), leading to activation of the DNA damage response (DDR) and DSB repair pathways. In most eukaryotes, telomeres, the specialized nucleoprotein structures at the chromosome termini, enforce chromosomal end stability through the activity of telomere-associated factors that inhibit activation of the DDR. These telomere-associated factors also play a crucial role in regulating the access and activity of the reverse transcriptase telomerase, which replenishes terminal telomeric repeats. In vertebrates, the shelterin complex, comprised of the TRF1, TRF2, RAP1, TIN2, TPP1 and POT1 proteins, plays an integral role in both of these functions (1-6).

TIN2 is a central component of shelterin, linking the double stranded telomeric binding proteins, TRF1 and TRF2, to the single stranded telomeric binding protein POT1 via its interaction with TPP1 (7). Additionally, TIN2 interacts with the cohesin subunit SA1 (8). Whereas murine cells express a single TIN2 isoform, which is important for the protection of telomeres from DNA damage signaling and fusions via classical- and alternative-non-homologous end joining pathways (9), both a short (TIN2S) and long (TIN2L) isoform of TIN2 are expressed in human cell lines (10) (Fig. 1A). TIN2L contains all 354 amino acids (aa) present in the shorter isoform along with an additional 97 aa at the C terminus via alternative splicing. Detailed interaction studies published to date have focused on residues shared between TIN2S and TIN2L or the full length TIN2S isoform. For example, of the TIN2 crystal structures that have been

64 reported, the first set consists of a small central peptide spanning aa 256-276, which
65 includes a TRF homology (TRFH) domain binding motif (TBM), in complex with the
66 TRF1- or TRF2- TRFH domains (9). The second set consists of the N terminal domain
67 of TIN2 (aa 2-202), which structurally resembles a TRFH domain, in a ternary complex
68 with TPP1- and TRF2-TBMs (11). While the TIN2-TBM interacts with TRF2 with a much
69 lower affinity than the TIN2-TRFH domain does, *in vivo* studies with TIN2S have
70 demonstrated that residues within the TIN2-TBM can mediate a weak interaction with
71 TRF2 when the interaction between the TIN2-TRFH and TRF2 is disrupted.
72 Interestingly, in contrast to its interaction with the TRF2-TRFH domain, the TIN2-TBM
73 interacts with a high affinity with the TRF1-TRFH domain and disruption of these
74 residues in TIN2S has profound impact on TIN2S-TRF1 interactions *in vivo* (9). Whether
75 the C-terminal TIN2L-extension influences TIN2's interaction with its shelterin binding
76 partners has not been determined. Similar to the interaction studies, little is known
77 regarding the functional contributions of TIN2L versus TIN2S at telomeres.
78 Simultaneous loss of both TIN2 isoforms via knockdown has seemingly contradictory
79 effects on telomerase regulation, due to destabilizing effects on TRF1, which is a
80 negative regulator of telomere length (12), and decreased telomere association of
81 TPP1, which is crucial for the recruitment of telomerase to the telomere (13).

82 Gene mutations associated with human disease often provide insight into
83 previously unrecognized protein function, which may be true for TIN2. *TINF2*, the gene
84 that encodes TIN2, is the second most commonly mutated gene in the telomere biology
85 disorder dyskeratosis congenita (DC) (14, 15). DC is a complex syndrome characterized
86 by bone marrow failure and cancer predisposition, pulmonary fibrosis, and a multitude

87 of other clinical features. Underlying these medical problems are constitutionally very
88 short telomeres (16). DC-associated *TINF2* mutations are most frequently *de novo*, yet,
89 strikingly result in drastically short telomeres within a single generation (15). This is in
90 contrast to autosomal dominant mutations in *TERT*, the catalytic component of
91 telomerase, or *TERC*, the integral RNA, which are most often inherited and result in
92 progressively shorter telomeres and increasing disease severity or multisystem
93 involvement in successive generations (17, 18). The basis for this rapid telomere
94 shortening remains to be fully elucidated. Notably, all *TINF2* mutations reported in
95 patients with very short telomeres, whether missense, frameshift, or nonsense, map to a
96 central 30 amino acid region (residues 269-298, DC-cluster), which is immediately C-
97 terminal to the TIN2-TBM and present in both TIN2S and TIN2L (8, 19-21) (Fig. 1A).
98 While the most N terminal truncation was shown to decrease TIN2S binding to TRF1,
99 no universal effect of these mutations on TIN2S binding to TRF1, TRF2, or TPP1 has
100 been observed (22, 23). Thus, it has been suggested that the impact of the TIN2
101 mutations could be on other interactions.

102 Consistent with this, TIN2 binds heterochromatin protein 1γ (HP1γ) via a binding
103 motif within the DC-cluster region (TIN2 residues 283-287) (24). HP1γ binds to H3 tails
104 methylated at lysine 9 and, similar to TIN2 (8), is necessary for sister telomere cohesion
105 (24). Some DC-associated mutations affect both HP1γ binding and sister telomere
106 cohesion, leading to the proposal that DC-associated mutations cause decreased sister
107 telomere cohesion, resulting in a loss of telomere lengthening via homologous
108 recombination during embryogenesis. However, frameshift/nonsense mutations C-
109 terminal to this binding motif would not be expected to reduce HP1γ binding, as was

110 observed for the Q298Rfs mutation. Notably, missense mutations have only been found
111 from residues 280-291, while frameshift and nonsense mutations have been found
112 throughout this region. These frameshift and nonsense mutations would obliterate any
113 specific functions of the C-terminal region of TIN2S and TIN2L and could result in the
114 expression of a truncated protein lacking the TIN2L C-terminal domain, as has been
115 shown for two such mutations (22). Our identification of a young child with DC, very
116 short telomeres and an even more C-terminal K302Rfs mutation further raises the
117 question of functions other than HP1γ binding contributing to the very short telomeres
118 observed in these patients.

119 Additionally, it has been reported that while DC-associated *TINF2* mutations do
120 not affect overall telomerase activity, they do result in decreased telomerase activity
121 immunoprecipitated with TIN2S (25). However, a mouse model in which a DC-
122 associated *TINF2* mutation results in decreased telomere length even in the absence of
123 the telomerase RNA component (26) indicates that defects in telomerase recruitment
124 alone are unlikely to account for the much more severe phenotype seen in patients with
125 *TINF2* mutations.

126 Importantly, both TIN2L and TIN2S contain all known binding regions and the
127 DC-cluster (10). Functions that may be unique or specific to TIN2L at the telomere and
128 any effects of DC-associated mutations on those functions remain unexamined. We
129 hypothesized that TIN2L has roles at the telomere not shared with the shorter isoform,
130 and that those roles could be impacted upon by DC-associated mutations. Herein, we
131 have identified differences in the ability of TIN2L and TIN2S to interact with TRF1 and
132 TRF2, and a role for the DC-cluster and phosphorylation specifically in TIN2L

133 interactions. Additionally, we show that TIN2L and TIN2S overexpression have different
134 effects on telomere length. These data suggest that TIN2S and TIN2L have differing
135 roles within the shelterin complex and in telomere regulation, and that the composition
136 of the shelterin complex could be fundamentally altered in patients with DC-associated
137 *TINF2* mutations.
138

139 **MATERIALS AND METHODS**

140 *Comparative analysis of protein sequences*

141 We used a real-value ET method (27) to assign a score to the degree of conservation of
142 protein residues from TIN2 orthologs reported by the Ensembl database (28). A BLAST
143 search against the NCBI's RefSeq (29) database, using the TIN2L sequence as the
144 query, was performed to confirm results from the Ensembl database. We chose to base
145 our analysis on mammalian sequences only, as Ensembl did not report any TIN2
146 orthologs in vertebrates other than mammals and amphibians, and the BLAST search
147 returned only mammalian sequences with matches to the last three exons of TIN2.

148 *Prediction of TIN2 phosphorylation and kinase-specific predictions*

149 Human TIN2L sequence (Uniprot identifier Q9BSI4-1) was analyzed using NetPhos3.1
150 (30, 31), GPS3.0 (32), and PPSP (30) algorithms via their respective servers
151 (http://gps.biocuckoo.org; http://www.cbs.dtu.dk/services/NetPhos/;
152 http://ppsp.biocuckoo.org/; each accessed November 18, 2017).

153 *Vectors and mutagenesis*

154 The pcDNA3.1-flag-2xHA-TIN2S and pcDNA-flag-2xHA-TIN2S-R282H vectors have
155 been previously described (22). The cDNA encoding the C terminus of TIN2L was

156 amplified from MGC-12628 (ATCC) and subcloned 3' to the penultimate codon in
157 pcDNA3.1-flag-2xHA-TIN2S to generate pcDNA3.1-flag-2xHA-TIN2L. pcDNA3.1-flag-
158 2xHA-TIN2L-R282H, pcDNA3.1-flag-2xHA-TIN2L-D391K+D395K, and pcDNA3.1-flag-
159 2xHA-TIN2L-DEEE(397-400)KKKK were generated using site directed mutagenesis as
160 previously described (22). pLenti6.3-GFP, pLenti6.3-TIN2S, pLenti6.3-TIN2L, pLenti6.3-
161 TIN2L-S396A, and pLenti6.3-TIN2L-S396E were generously provided by Dr. Kenneth
162 Scott (Baylor College of Medicine). The C termini of TIN2L-S396E and TIN2L-S396A
163 were amplified from their respective pLenti6.3 vectors and subcloned 3' to the
164 penultimate codon in pcDNA3.1-flag-2xHA-TIN2S to generate pcDNA3.1-flag-2xHA-
165 TIN2L-S396E and pcDNA3.1-flag-2xHA-TIN2L-S396A. pLenti6.3-TIN2S-R282H was
166 generated from pcDNA3.1-flag-2xHA-TIN2S-R282H via subcloning. pcDNA3.1-flag-
167 2xHA-TIN2L-R282H+S396A was generated via subcloning from plasmids containing the
168 respective mutations. myc-TPP1 was amplified from pLpcx-myc-TPP1 (generously
169 provided by Dr. Susan Smith, NYU) and subcloned into pcDNA3.1 to generate
170 pcDNA3.1-myc-TPP1. TIN2L was amplified from pcDNA3.1-flag-2xHA-TIN2L and
171 subcloned into pET28SUMO (generously provided by Dr. Ming Lei, University of
172 Michigan) to generate pET28SUMO-TIN2L. TIN2L, TIN2L-D391K+D395K, and TIN2L-
173 R282H were amplified from their respective pcDNA3.1 vectors and subcloned into
174 GCN4 leucine zipper-Venus 2 (C-terminal half; V2) to generate TIN2L-V2, TIN2L-
175 D391K-V2, and TIN2L-R282H-V2. V1-TRF2 and V2-RAD21 have been previously
176 described (2). pcDNA3.1-myc-TRF1, pcDNA3.1-myc-TRF2, pcDNA3.1-myc-TRF2-
177 F120A, and pSP73Sty11 were all a generous gift from Dr. Titia De Lange (Rockefeller
178 University).

179 *Immunoblotting*

180 Cells were resuspended in ice cold lysis buffer (50 mM Tris-HCl at pH 7.5, 1 mM EDTA,
181 400 mM NaCl, 1% Triton X-100, 0.1% SDS, 1 mM DTT, 1 mM PMSF and 1X protease
182 inhibitor cocktail III [Calbiochem]) and incubated for 10 minutes on ice prior to addition
183 of an equal amount of ice cold water. The lysates were then centrifuged at 4 ˚C and
184 20,800 x g for 10 minutes, and the pellet was discarded. Protein concentration was
185 determined using the BCA protein assay kit (Pierce). Lysates were resolved on 10%
186 SDS-polyacrylamide gels and transferred to nitrocellulose membranes. The membranes
187 were probed with at least one of these primary antibodies as indicated in the text: rabbit
188 polyclonal α-FLAG (Sigma-Aldrich), rabbit polyclonal α-c-Myc (Sigma-Aldrich), rabbit
189 polyclonal α-TIN2 #865 (kindly provided by Dr. Titia De Lange, Rockefeller University),
190 mouse monoclonal α-β-actin (Sigma-Aldrich), rabbit polyclonal α-TRF1 (Santa Cruz),
191 rabbit polyclonal α-TRF2 (Santa Cruz), rabbit polyclonal α-POT1 (Abcam), or rabbit
192 polyclonal α-GFP (Abcam). The appropriate IRDye 800CQ conjugated secondary
193 antibody (Li-Cor) was then used and blots were visualized using the Li-Cor Odyssey
194 Infrared Imaging System. Blots were stripped by incubation in 0.1 M NaOH for 10
195 minutes at room temperature and reprobed. Immunoblots were quantified using
196 Odyssey v3.0 Software (Li-Cor).

197 *Phosphate affinity SDS-PAGE using Phos-tag™*

198 Lysates were prepared as described above for immunoblotting, with the addition of 1x
199 Phosphatase Inhibitor Cocktail II (Sigma-Aldrich) to the lysis buffer to prevent
200 dephosphorylation. As a control, protein extracts were also prepared in the absence of
201 phosphatase inhibitors and treated with 400 U of λ phosphatase (NEB) for 30 minutes

202 at 30 °C. Lysates were resolved on a 10% w/v acrylamide gel with 100 μM Phos-tag^{TM}

203 (Wako) prepared according manufacturer's instructions. Prior to transfer, the gel was

204 soaked in transfer buffer with 1 mM EDTA for 10 minutes at room temperature with

205 shaking. Subsequent steps were carried out as described above for immunoblotting.

206 *TIN2L protein purification*

207 Protein purification was conducted similarly to previously described for TIN2S, with

208 slight modifications (9). Human TIN2L in a modified pET28b vector with a SUMO site

209 between the 6Xhis tag and the N terminus of TIN2L was expressed in BL21(DE3) *E.*

210 *coli.* Following induction with 0.1 mM IPTG, cells were grown for 24 hours at 16 °C and

211 then harvested by centrifugation. Cells were then resuspended in lysis buffer (50 mM

212 phosphate buffer pH 7.2, 0.5 mM 2-mercaptoethanol, 10% glycerol, 1 mM PMSF, 400

213 mM NaCl, 3 mM imidazole, 0.1 mg/mL lysozyme, 1X protease inhibitor cocktail set III

214 [Calbiochem]) and lysed via sonication. The lysate was then cleared via centrifugation,

215 and incubated overnight at 4 °C with Ni-NTA agarose beads (Qiagen). The bead-lysate

216 slurry was applied to a column and washed with 10 column volumes of wash buffer (50

217 mM phosphate buffer pH 7.2, 0.5 mM β-mercaptoethanol, 10% glycerol, 1 mM PMSF,

218 400 mM NaCl, 20 mM imidazole) prior to addition of 1.5 column volumes of elution

219 buffer (50 mM phosphate buffer pH 7.2, 0.5 mM β-mercaptoethanol, 10% glycerol, 1

220 mM PMSF, 400 mM NaCl, 250 mM imidazole, 1X protease inhibitor cocktail set III

221 [Calbiochem]). The eluate was then concentrated using an Amicon Ultra 10K

222 Centrifugal filter (Millipore) prior to separation on a HiLoad 16/600 Superdex 200 pg (GE

223 Healthcare Life Sciences) gel filtration column equilibrated with gel filtration buffer (25

224 mM Tris pH 8.0, 150 mM NaCl, 5 mM DTT). The fractions containing TIN2L were

225 pooled, concentrated using an Amicon Ultra 10K Centrifugal filter (Millipore), and stored
226 at -80 °C until use.

227 *In vitro phosphorylation*

228 Three micrograms of recombinant TIN2L purified from *E. coli* was incubated with 10 U
229 of CK2 (NEB) and 10 μCi γ^{32}P-ATP in 1X CK2 reaction buffer (NEB) at 30°C for 30
230 minutes. As a control, 3 μg of BSA (NEB) was incubated with CK2 under the same
231 conditions. To confirm that the observed phosphorylation was carried out by CK2, the
232 reaction was also performed in the presence of increasing concentrations of 4,5,6,7-
233 Tetrabromo-2-azabenzimidazole (TBB), a CK2 inhibitor. Following the phosphorylation
234 reaction, proteins were resolved on a 10% SDS-PAGE gel, which was then exposed to
235 a PhosphorImager screen. *In vitro* phosphorylation assays were also performed using
236 flag tagged TIN2L or TIN2L-S396A partially purified from 293T cells. Twenty four hours
237 after transfection with 5 μg of DNA using lipofectamine and Plus (Invitrogen) according
238 the manufacturer's instructions, cells were lysed as described above. Phosphatase
239 inhibitor cocktail II (Sigma-Aldrich) was added to one quarter of the lysate, which was
240 set aside as a control. The remainder of the lysate was treated with 400 U of λ
241 phosphatase (NEB) for 30 minutes at 30°C. The phosphatase was then inactivated by
242 the addition of 50 mM EDTA and 1X phosphatase inhibitor cocktail II (Sigma-Aldrich).
243 The lysates, including the reserved control, were then incubated overnight at 4 °C with
244 mouse monoclonal α-FLAG M2 magnetic beads (Sigma-Aldrich) to isolate flag tagged
245 TIN2L or TIN2L-S396A. Beads were washed four times with a 1:1 dilution of lysis buffer,
246 and then resuspended in 1X CK2 buffer (NEB) supplemented with 200 μM ATP, 1X

247 phosphatase inhibitor cocktail II (Sigma-Aldrich), 1X protease inhibitor cocktail III
248 (Calbiochem) and the indicated amount of CK2. Phosphorylation was carried out at 30
249 °C for 30 minutes, prior to analysis using phosphate affinity SDS-PAGE with Phos-
250 tag™.

251 *Co-immunoprecipitation*

252 Co-immunoprecipitations were conducted similarly to previously described (7). For TIN2
253 co-immunoprecipitations with TRF1, TRF2, or TPP1, 3 x 10^6 HEK 293T cells were co-
254 transfected with 5 μg of each plasmid using the lipofectamine and Plus reagents
255 (Invitrogen) according to the manufacturer's instructions. Twenty four hours after
256 transfection, the cells were lysed as described above for immunoblotting. Half a percent
257 of the supernatant was reserved as input. Supernatants were incubated overnight at 4
258 °C with 60 μL of mouse monoclonal α-FLAG M2 magnetic beads (Sigma-Aldrich) or 2
259 μg mouse monoclonal α-Myc 9E10 (Abcam). For myc pull downs, 60 μL of Protein G
260 Plus-agarose beads (Calbiochem) were added during the final hour. Beads were
261 washed four times with a 1:1 dilution of lysis buffer prior to elution with Laemmli loading
262 buffer. Proteins were analyzed by immunoblotting. Western blots were quantified using
263 Odyssey V3.0 (LiCor).

264 *Protein complementation assay*

265 The protein complementation assay was carried out as previously described (2).

266 *Stable overexpression cell lines*

267 HT1080 cells were infected with pLenti6.3-GFP, pLenti6.3-TIN2S, pLenti6.3-TIN2S-
268 R282H, pLenti6.3-TIN2L, pLenti6.3-TIN2L-S396A, or pLenti6.3-TIN2L-S396E lentivirus
269 produced in HEK293T cells. HT1080 cells overexpressing the genes of interest were
270 then selected by incubation with selection media containing blasticidin. Beginning two
271 weeks after initial viral induction (time point 0), cells were counted and plated every 3-4
272 days to follow growth and population doublings, and cells pellets were saved at -80 °C
273 for further analysis.

274 *Measurement of telomere length*

275 Measurement of bulk telomere terminal restriction fragment length was determined by
276 Southern blotting as previously described (33) with the following specifications.
277 Genomic DNA was isolated using the DNeasy Blood and Tissue kit (Qiagen) and
278 subjected to digestion with *Hinf*I, *Rsa*I, and RNase A (NEB). Digested DNA was
279 separated on a 1% agarose gel via pulse field gel electrophoresis and then transferred
280 to a Zetaprobe GT Membrane (Bio-Rad) for detection of telomeric sequence by
281 hybridization with an 800 bp telomeric probe derived from pSP73Sty11 fragment labeled
282 with α^{32}P-dCTP using Klenow fragment (34). Telomere length was determined using
283 ImageQuant software (GE Healthcare Life Sciences) and Telorun
284 (http://www4.utsouthwestern.edu/cellbio/shay-wright/research/sw_lab_methods.htm).
285 Single telomere length analysis (STELA) at 17p and XpYp was performed as
286 previously described (35).

287 *CRISPR/Cas9 cell line creation*

288 Guide RNAs (gRNAs) targeting exons 7 and 8 of the *TINF2* locus were designed using
289 the CRISPR Design tool (http://crispr.mit.edu/) (36). Three guides with quality scores of
290 76 or greater were chosen. Cleavage efficiency of the gRNAs was determined using the
291 Guide-it mutation detection kit (Takara) according to manufacturer's instructions.
292 HT1080 and Flp-In T-REx cell lines were transfected with 5 μg of pGS-gRNA-Cas9-
293 Puro (Genscript) containing the desired gRNA using lipofectamine and Plus (Invitrogen)
294 according to the manufacturer's instructions. Two days after transfection, the host cell
295 line was diluted and plated to form colonies. After expansion of the clones, 48 colonies
296 from each gRNA were screened for mutations in the *TINF2* gene initially by sequencing
297 PCR products amplified from the surrounding genomic region. Those with products with
298 abnormal sequences were TopoTA cloned and 10 TopoTA clones sequenced to
299 determine the sequences on each allele. Cells from colonies of interest were counted
300 and plated every 3-4 days to follow growth and population doublings, and cell pellets
301 were saved at -80 °C for further analysis.

302 *Isolation of endogenous nuclear complexes*

303 HeLa cell nuclear complexes were examined as previously described (37). Briefly,
304 nuclei from 7×10^9 HeLa cells were extracted using 0.5 M KCl (38). Extracts were
305 dialyzed into S-300 buffer (50 mM Tris pH 7.5, 150 mM KCl, 0.2 mM EDTA, 0.025%
306 NP-40, 0.5 M dithiothreitol, 1X cOmplete protease inhibitor [Roche]) and clarified by
307 centrifugation. The dialyzed sample was concentrated using an Amicon Ultra 10K
308 Centrifugal filter (Millipore) prior to fractionation on a HiLoad 16/600 Superdex 200 pg
309 (GE Healthcare Life Sciences) gel filtration column equilibrated with S-300 buffer. Half

310 milliliter fractions were taken beginning at 30 mL elution volume and analyzed by
311 immunoblotting.

312 *Telomere chromatin immunoprecipitation*

313 Cells were fixed in 1% formaldehyde for 30 minutes at room temperature followed by
314 lysis in RIPA buffer (50 mM Tris-HCl at pH 8, 5 mM EDTA, 150 mM NaCl, 0.5% sodium
315 deoxycholate, 1% NP-40, 0.1% SDS, 1 mM PMSF and 1X protease inhibitor cocktail III
316 [Calbiochem]). The lysates were sonicated in a Diagenode Bioruptor for 10 minutes, 3
317 times at high setting to generate ~1 kb DNA fragments. Cellular debris was pelleted by
318 centrifugation at 4 ˚C and 20,000 g for 10 minutes, and the protein concentration
319 assessed using the BCA protein assay kit (Pierce). For immunoprecipitation 600 µg of
320 the lysate was incubated with the corresponding antibodies (3 µg) overnight at 4 °C:
321 rabbit α-TRF2 (Novus, NB110-57130), rabbit α-TRF1 (Abcam, ab1423), rabbit IgG
322 (Santa Cruz). The next day, 45 µl of protein G magnetic beads (Pierce) were added and
323 after 2 hours, the beads were washed 2X in RIPA buffer, 4X in wash buffer (100 mM
324 Tris-HCl pH 8.5, 500 mM LiCl, 1% NP-40, 1% sodium deoxycholate) and another 2X in
325 RIPA buffer. Following two washes in 1X TE, proteins were eluted in 1XTE/1% SDS and
326 incubated in 65 °C overnight to reverse the crosslinks. The samples were then treated
327 with RNase A (20 µg) and Proteinase K (40 µg) and subjected to phenol-chloroform
328 extraction. After ethanol precipitation, dot blotting was performed on a Zeta-probe
329 membrane (Bio-Rad) to hybridize the DNA with an 800 bp radiolabeled TTAGGG probe
330 to assess the amount of immunoprecipitated telomeric DNA. A 5′ α^{32}P-labeled
331 oligonucleotide Alu probe was used as negative control. ImageQuant software was

332 used to quantify the signal intensity of telomeric or Alu IP relative to the corresponding
333 input signals.

334 *Cell line authentication*

335 Cell lines were authenticated by short tandem repeat DNA analysis at MD Anderson
336 Cancer Center Characterized Cell Line Core Facility (September 1, 2017).

337 RESULTS

338 **TIN2L is phosphorylated by casein kinase 2 (CK2).** To examine whether TIN2L
339 contains regions potentially important for function that are not present in the more
340 commonly studied shorter isoform (TINS), we first estimated conservation of residue
341 types across mammalian orthologs of TIN2L (see Materials and Methods). The
342 estimated degree of conservation is collated in Figure 1A below the approximate or
343 delineated TIN2 binding regions determined previously by crystallography, yeast two
344 hybrid, far-western, and co-immunoprecipitation experiments (7, 8, 19, 20). While much
345 of the TIN2 sequence is highly variable, we found conserved regions are present and
346 some coincide with the known interaction regions of TIN2. In particular, region 258 to
347 267, which contains the TBM and is sufficient for high affinity TRF1 but not TRF2
348 interaction (9), consists almost entirely of residues that are identical across all
349 mammalian sequences. A large fraction of the residues within the N terminal TRFH
350 domain are also highly evolutionarily constrained. Lastly, within the 30 aa region
351 spanning residues 269 to 298, where all of the DC-associated TIN2 mutations have
352 been reported to date (indicated as DC in Fig. 1A), only residues 280 to 291 showed
353 signs of evolutionary constraint, coinciding with the HP1γ binding motif (residues 283-

354 287). In addition to the evolutionary constraint in these regions shared by TIN2S and
355 TIN2L, we identified two highly evolutionarily constrained regions within the C-terminal
356 domain exclusive to TIN2L (TIN2L CTD) (Fig. 1A). The region consisting of residues
357 388-400 was the more highly constrained of the two.

358 Within this region are residues 396SDEE399, which conform to a casein kinase 2 (CK2)
359 recognition motif (S/T-X-X-E/D, where X represents non-basic residues) targeting
360 phosphorylation of S396 (39, 40). The prediction for S396 phosphorylation and its
361 phosphorylation by CK2 was robust across several protein phosphorylation prediction
362 algorithms including NetPhos3.1 (30, 31), GPS3.0 (32), and PPSP (30). These residues
363 were conserved across mammalian orthologs reported in the Uniprot database (Fig.
364 S1). Further supporting these data, endogenous TIN2L was previously found to be
365 phosphorylated at S396 in human embryonic stem cells using high throughput mass
366 spectrometry (41). Unlike humans, mice express only one isoform of TIN2 (10). Mouse
367 TIN2 includes a C-terminal region with high similarity to the C-terminal extension in
368 human TIN2L, and the cognate residue to human S396, mouse S380, was also found to
369 be phosphorylated in three separate mass spectrometry analyses (42-44).

370 CK2 is known to phosphorylate TRF1 (45). This phosphorylation of TRF1 is necessary
371 for its stability, binding to telomeric DNA, and homodimerization, thereby contributing to
372 the negative length regulation of telomeres. Because CK2 is important for the telomeric
373 function of TRF1 and a putative CK2 phosphorylation site is present in TIN2L, we asked
374 if TIN2Lis phosphorylated and, if so, by CK2. To determine if TIN2L is phosphorylated,
375 we utilized the reagent Phos-tag^{TM}, which retards the migration of phosphorylated
376 proteins through SDS-polyacrylamide gels (46). First, we analyzed transiently

377 expressed, tagged proteins in HEK 293T cells and found that TIN2L migrated more
378 rapidly through the gel following λ phosphatase treatment, indicating that the majority of
379 TIN2L was phosphorylated (Fig. 1B). While TIN2S can be phosphorylated (47), the
380 migration of TIN2S was unaffected by λ phosphatase treatment, indicating that this
381 isoform is not predominantly phosphorylated in asynchronous cells (Fig. 1B) Charge
382 swapping mutations in the CK2 recognition site (D391K+D395K and DEEE397-
383 400KKKK) and mutation of S396 to either a phosphomimetic (S396E) or phosphodead
384 (S396A) residue abolished TIN2L phosphorylation (Fig. 1C). The most common
385 missense mutation in DC, R282H, did not affect TIN2L phosphorylation (Fig. 1C).

386 CK2 is an essential kinase. Inhibition of CK2, via either RNA interference or the CK2-
387 selective chemical inhibitor TBB, results in apoptosis, making it difficult to study
388 phosphorylation by CK2 in an endogenous context (48). To overcome this and establish
389 whether CK2 might be responsible for the observed TIN2L phosphorylation, we purified
390 recombinant tagged TIN2L from *E. coli* and determined the ability of recombinant CK2
391 purified from *E. coli* (NEB, Fig. 1D) to phosphorylate this TIN2L *in vitro*. TIN2L was
392 phosphorylated by CK2 in the presence of [γ^{32}P]-ATP, as indicated by the presence of
393 radiolabeled TIN2L (Fig. 1E). This phosphorylation decreased in the presence of TBB,
394 which drastically inhibits CK2 but not 33 other kinases (49), indicating that TIN2L
395 phosphorylation was CK2 dependent. To determine if the residue phosphorylated by
396 CK2 was S396, we overexpressed TIN2L or TIN2L-S396A in 293T cells, treated the cell
397 lysates with λ phosphatase to remove any existing phosphorylations, partially purified
398 TIN2 via immunoprecipitation, and then incubated it with recombinant CK2.
399 Phosphorylation status was then determined using SDS-PAGE in the presence of Phos-

400 tag^{TM}, followed by western blotting. Immunoprecipitated TIN2L not subjected to λ
401 phosphatase treatment was prepared as a control. As shown in Figure 1F, wild type
402 TIN2L was phosphorylated by CK2, while TIN2L-S396A was not. In summary, these
403 data showed highly conserved residues corresponding with a CK2 recognition site in
404 TIN2L, loss of phosphorylation of tagged expressed TIN2L upon mutation of the site in
405 cells, *and in vitro* phosphorylation of wild type, but not mutant, partially purified TIN2L by
406 CK2 and which was reduced by a highly specific CK2 inhibitor. Combined with the
407 previous mass spectrometry data indicating S396 is phosphorylated in both mouse and
408 human cells, this data strongly supports the notion that TIN2L-S396 is phosphorylated
409 by CK2 *in vivo*.

410 **The DC cluster and TIN2L phosphorylation enhance TIN2L's association with**
411 **TRF2 *in vivo*.** To determine the molecular effects of TIN2L phosphorylation, we
412 examined the ability of transiently expressed epitope tagged TIN2L to interact with the
413 known TIN2S shelterin binding partners, which were also transiently expressed and
414 epitope tagged, and the effect of mutation of the phosphorylation site on those
415 interactions via co-immunoprecipitation. We also compared TIN2L interactions with that
416 of TIN2S and the effect of the DC R282H mutation on TIN2L as compared to TIN2S
417 interactions. Interestingly, TIN2L interacted much more robustly with TRF2 than TIN2S
418 (Fig. 2A, quantified in Fig. 2D). This is in contrast to what was previously published (10).
419 However, as shown in Figure 2D, this result was very reproducible with consistent
420 results across multiple biological replicates. As previously reported, the most common
421 missense mutation in TIN2 in DC patients, R282H, had no effect on TIN2S binding to
422 TRF2 (Fig. 2A, quantified in Fig. 2D) (22, 23, 26). In contrast, the R282H mutation

423 reduced TIN2L binding to TRF2 to levels similar to that of wild type TIN2S, indicating an
424 effect of the DC cluster that is manifest only within the context of the long isoform.
425 Similarly, the phosphodead mutation greatly reduced TIN2L binding to TRF2, while the
426 phosphomimetic mutation did not, indicating that TIN2L phosphorylation at S396 is
427 critical for this enhanced interaction (Fig. 2B, quantified in Fig. 2D). The double mutant
428 TIN2L-R282H+S396A did not decrease TRF2 binding beyond either mutation alone,
429 indicating that the DC-cluster and TIN2L phosphorylation site cooperate to enhance
430 TRF2 binding to TIN2L (Fig. 2C, quantified in Fig. 2D).

431 The importance of S396 phosphorylation and R282 in TIN2L-TRF2 interaction was also
432 observed using the protein-fragment complementation assay (PCA), with TIN2L and
433 TRF2 fused with the C- (denoted as V2) and N- (denoted as V1) terminal halves of the
434 Venus yellow fluorescent protein variant, respectively. In this type of PCA, fluorescence
435 is only detected when the proteins to which the split Venus halves are tagged come into
436 close proximity, allowing reconstitution of N- and C-terminal fragments of the Venus
437 yellow fluorescent protein (50). The fluorescence observed with co-transfection of
438 TIN2L-V2 with V1-TRF2 was markedly reduced with the TIN2L-R282H-V2 and TIN2L-
439 D391K+D395K-V2, which abolishes TIN2L phosphorylation (Fig. 1C), mutants (Fig. 3),
440 consistent with a decreased interaction of these TIN2L mutants with TRF2. We found
441 expression of TIN2S and TIN2L differed greatly in these constructs, so the interaction
442 between the TIN2 isoforms and TRF2 could not be compared using PCA.

443 We next determined if the increased interaction of TRF2 with TIN2L involves the TRF2
444 TRFH domain. To do this, we employed a TRF2 TRFH domain mutation, F120A. TRF2-
445 F120A was shown previously by transient transfection and co-immunoprecipitation to

446 have no impact on TIN2S's interaction with TRF2, whereas mutation of the cognate
447 residue in the TRF1 TRFH domain, F142A, drastically reduced TIN2S's interaction with
448 TRF1. Nonetheless, the conformations of the TIN2-TBM bound to the TRFH domains of
449 TRF1 and TRF2 are similar (9) and, in one study, TRF2-F120A was been shown to
450 reduce transiently transfected TRF2's ability to interact with endogenous TIN2, although
451 it was not determined if this was TIN2S or TIN2L (51). Reproducibly in our assays and
452 in contrast to what was observed by transient transfection and co-immunoprecipitation
453 for TRF2-F120A and TIN2S, we found that the TRF2-F120A mutation decreased
454 TIN2L's binding to TRF2 (Fig. 4). This suggests that the CTD of TIN2L stabilizes the
455 TIN2-TBM - TRF2-TRFH interaction *in vivo*.

456 **TIN2L binds less robustly than TIN2S to TRF1 but equivalently to TPP1.** We next
457 examined how TRF1 interacted with TIN2L relative to TIN2S using transient expression
458 and co-immunoprecipitation. Conversely and in striking contrast to TRF2, TRF1
459 interacted much more robustly with TIN2S than TIN2L (Fig. 5A, quantified in Fig. 5B).
460 The R282H mutation had no effect on TIN2S binding to TRF1, but reduced TIN2L's
461 ability to bind TRF1 even further. However, TIN2L phosphorylation appeared to play no
462 role in interaction with TRF1 (Fig. 5A and B), unlike with TRF2 (Fig. 2B and D).

463 Lastly, having found that TRF2 interacted more robustly with TIN2L than TIN2S, and,
464 conversely, TRF1 interacted more robustly with TIN2S than TIN2L, we next examined
465 how the isoforms interacted with TIN2's third shelterin binding partner, TPP1. In
466 contrast to TRF1 and TRF2, we found both isoforms interacted at similar levels with
467 TPP1 in the co-immunoprecipitation assays (Fig. 5C, quantified in Fig. 5D).

468 To explore whether TIN2L is present in endogenous shelterin complexes, we subjected
469 the nuclear fraction from a HeLa cell lysate to size based fractionation under physiologic
470 ionic strength using a gel filtration column. As previously reported, endogenous TIN2S,
471 TRF1, TRF2, and POT1 co-fractionated over a range of molecular masses larger than
472 670 kDa (Fig. 6) (7, 37, 52), which is larger than the size of a core shelterin complex,
473 consisting of TIN2S, TRF2 homodimer, POT1, and TPP1 (306 kDa) (53), TRF1
474 homodimer (115 kDa) (53) and 2 RAP1 molecules (expected 88 kDa). TIN2L was also
475 present in these fractions, consistent with it being in a complex with the shelterin
476 components. Given the larger than expected cumulative size of the proteins that co-
477 fractionated, TIN2S and TIN2L could simultaneously be present within a single shelterin
478 complex.

479 **TIN2L is neither required for viability nor normal telomere length maintenance in**
480 **transformed cell lines.** Given the differences in shelterin component binding between
481 TIN2L and TIN2S, we next sought to determine if they might also differentially impact
482 telomere length regulation. The role of TIN2L S396 phosphorylation in telomere length
483 regulation was of particular interest given CK2's role in telomere length regulation via its
484 phosphorylation of TRF1 (37). First, we stably overexpressed TIN2S, TIN2S-R282H,
485 TIN2L, TIN2L-S396A, TIN2L-S396E or a GFP control in the HT1080 cell line and
486 determined the telomere length by Southern blot over successive population doublings
487 (Fig. 7). We found that the telomeres progressively elongated in the HT1080 GFP
488 control cells. Telomere elongation in this control cell line has been observed by others
489 (19, 21, 25, 26, 34), and may reflect resetting of telomere length in sublines that had
490 previously undergone stochastic shortening. While telomeres progressively elongated in

491 the GFP control cell lines, overexpression of either TIN2S or TIN2S-R282H inhibited
492 this progressive elongation, consistent with previous reports demonstrating impairment
493 of telomere maintenance upon TIN2S overexpression (24, 25). In contrast, telomeres
494 continued to progressively elongate in cells overexpressing wild type TIN2L, which was
495 a consistent observation in separately generated cell lines (Fig. 7 and S2). This result
496 could indicate that TIN2L simply lacks activity (as with GFP) or specifically lacks the
497 inhibitory activity of TIN2S. However, whereas telomeres also progressively elongated
498 in cells overexpressing TIN2L with the phosphomimetic S396E mutation, they did not in
499 cells overexpressing TIN2L with the phosphodead S396A mutation (Fig. 7 and S3). The
500 differences in telomere length changes could not be attributed to differences in levels of
501 overexpression, which were equivalent in each of the cell lines (Fig. 7C, S2, and S3) nor
502 to differences in population doubling time or cumulative population doublings for the cell
503 lines, which were equivalent (Fig. S4). Taken together, these results are most
504 consistent with the wild type TIN2L lacking inhibitory activity and the S396A mutation
505 resulting in TIN2L becoming TIN2S-like with respect to telomere length regulation,
506 similar to the effect it has on TIN2L's TRF2 binding (Figs. 2B and 2D).

507 To explore the role of endogenous TIN2L in telomere length regulation, we used the
508 CRISPR/Cas9 system (54) to modify the genomic *TINF2* locus. We designed guide
509 RNAs that targeted TIN2L-specific exons 7 and 8 for mutagenesis (Fig. S5A and B),
510 thereby creating cell lines that still encoded TIN2S, but either no longer encoded TIN2L
511 protein or encoded a protein that was truncated N-terminal to S396. We characterized
512 four unique compound heterozygous cell lines, three in the HEK 293-derived Flp-In T-
513 REx cell line and one in the HT1080 cell line (Fig. S5C). Clonal lines that were isolated

514 but found to not contain mutations in *TINF2* served as controls. The Flp-In T-REx lines
515 285-F3 and 285-F10 had frameshift mutations in exon 7 of each allele, whereas the cell
516 line 286-R had frameshift mutations in exon 8, N terminal to S396. The HT1080 lines
517 286-6A, 286-6B, and 286-6C, which were derived from the same clone, had an in frame
518 deletion of 15 bp, encoding a protein lacking amino acids 387-392, and a frameshift
519 mutation encoding a protein truncated at amino acid 394.

520 The TIN2L deficient clones were viable, although some clones exhibited decreased
521 growth compared to WT (Fig. S6). STELA analysis, which provides a sensitive measure
522 of changes in telomere length, revealed that the average 17p or XpYp telomere length
523 in independently derived clones varied within the range observed in clones with intact
524 TIN2L and over successive population doublings (Figs. 8 and S7). These results
525 suggest that in these telomerase-positive cancer (HT1080) and transformed (Flp-In T-
526 REx) cell lines, TIN2L is neither required for viability nor normal telomere length
527 maintenance.

528 In contrast to our approach, Kim et al., studied the effect of CRISPR/Cas9 knockout of
529 both TIN2 isoforms in HeLa cells (55). They found that loss of both TIN2 isoforms
530 results in a reduction in TRF2 but not TRF1 association with telomeres in chromatin
531 immunoprecipitation assays. Therefore, we determined the effect of loss of TIN2L
532 protein alone on the association of TRF2 with telomeres. Although TIN2L interacted
533 preferentially with TRF2 in co-IP experiments (Fig. 2), the absence of intact TIN2L
534 protein had no impact on the telomere association of TRF2 (Fig. 9). The interaction of
535 TRF1 with telomeres was similarly unaffected. Together with the telomere length data,

536 these results suggest that TIN2L and TIN2S have redundant functions in these cell
537 lines.

538 **DISCUSSION**

539 Prior studies have focused on the shorter isoform of TIN2, however, our data reveal
540 differences in the interactions of TIN2S and TIN2L with TRF1 and TRF2, suggesting
541 that the composition of the shelterin complex and the interactions within may be even
542 more complex than previously thought (7, 37, 53, 56). Although previous studies have
543 indicated that DC-associated mutations do not uniformly impact TIN2S interaction with
544 TRF1, TRF2 and TPP1 (22, 23), the impact of the most common DC-associated
545 mutation on TIN2L's ability to bind to both TRF1 and TRF2 leaves open the possibility
546 that the composition of the shelterin complex may be fundamentally altered in patients
547 with *TINF2* mutations, potentially contributing to their devastatingly short telomeres.

548 Herein, this study demonstrates that the increased interaction between TIN2L and
549 TRF2, in comparison to TIN2S, requires the residue most commonly mutated in DC,
550 R282, as well as phosphorylation of S396, and that R282 and phospho-S396 cooperate
551 or redundantly promote this enhanced interaction (Figs. 2 and 3). These findings were
552 unexpected as the primary TRF2 binding region in TIN2S resides within its N terminal
553 TRFH-domain (11, 20) and the most common mutation in DC has no effect on TIN2S-
554 TRF2 interaction (22, 23, 26). Additionally, we found that the TRF2-TRFH domain is
555 required for this increased interaction, which was similarly unexpected based on the
556 lack of impact of the TRF2-F120A mutation on TIN2S-TRF2 interaction *in vivo* (9). How
557 the TIN2L-specific C-terminal domain influences TRF2 binding remains to be

558 determined. As this region is predicted to be intrinsically disordered, structural studies
559 will likely prove challenging.

560 While overexpression of TIN2S inhibited progressive telomere elongation in HT1080
561 cells, overexpression of TIN2L did not (Figs. 7 and S3). It is interesting to consider the
562 possible mechanisms for this difference in light of protein-protein interaction data. It has
563 previously been shown that TIN2S prevents inactivation of TRF1 via inhibition of poly-
564 ADP ribosylation of TRF1 by tankyrase (12). TRF1 is a negative regulator of telomere
565 length (34). Since TRF1 interacts much more robustly with TIN2S than TIN2L (Fig. 5A
566 and B), the discrepancy in telomere length maintenance could be due to effects on
567 TRF1. Overexpression of TIN2L with a phosphodead mutation also inhibited
568 progressive telomere elongation (Figs. 2 and S3). If the failure of telomeres to elongate
569 in cells overexpressing TIN2S is indeed due to TRF1 stabilization, this is unlikely to be
570 the mechanism for TIN2L-S396A mediated failure of telomere elongation, since TIN2L
571 wild type and S396A interacted with TRF1 at similar levels (Fig. 5A and B). It is
572 therefore possible that phosphorylated TIN2L has a role in telomere maintenance
573 unique from either TIN2S or unphosphorylated TIN2L.

574 When endogenous full length TIN2L was eliminated using the CRISPR/Cas9 system, no
575 consistent effect on telomere length was observed, which was surprising given the
576 highly conserved CK2 consensus site within this region. While it is possible that TIN2S
577 and TIN2L have redundant functions in telomere length maintenance, it is equally
578 possible that TIN2L has other roles in telomere function. For example, we found TIN2L
579 interacts with TRF2 via F120 (Fig. 4), a residue within its TRFH domain that is known to
580 be critical for TRF2 binding to Apollo and SLX4 (9, 57). We speculate that TIN2L may

581 compete with these or other proteins that bind TRF2 via the TRFH domain. Therefore,
582 in patients with the R282H mutation, the reduced interaction of TIN2L with TRF2 could
583 result in a reduction in TIN2L binding to TRF2 at the telomere, thereby allowing
584 increased recruitment of Apollo (58), SLX4 (57) or other factors that may drive telomere
585 shortening. Future studies will address this hypothesis.

586 Due to the difficulties in exploring the interactions of each isoform and multiple
587 mutations with TRF1, TRF2 and TPP1 in an endogenous setting, these results were
588 obtained using a transient transfection system with epitope tagged proteins expressed
589 at higher than endogenous levels. The use of epitope tagging of TIN2S and TIN2L was
590 necessary as any antibody designed to bind TIN2S would also, by necessity, bind to
591 TIN2L. This may raise concern that the differential interactions are directly or indirectly
592 the result of the overexpression. However, using the same set of constructs expressed
593 at the same level under identical conditions in both co-IP and PCA, we observed
594 isoform- and allele-specific effects that suggest targeted impact on protein interaction.
595 TIN2S and TIN2L interacted similarly with TPP1 and the interaction was not impacted
596 by either R282H or S396A. Yet we observed very specific results with TIN2S and TIN2L
597 interactions with TRF1 and TRF2, and very specific effects of R282H or S396A on
598 TIN2S and TIN2L interactions. This suggests the differential interactions observed were
599 unlikely to be due to nonspecific effects such as aggregation.

600 This study indicates that the two TIN2 isoforms preferentially interact with different
601 members of the shelterin complex. We therefore anticipate that they could play different
602 roles in telomere regulation. These data indicate that the most common DC-associated
603 *TINF2* mutation greatly affects the ability of TIN2L, but not TIN2S, to interact with

604 members of the shelterin complex. While the field has largely overlooked the longer
605 isoform of TIN2, future studies will need to take both isoforms into account.

606 **ACKNOWLEDGEMENTS**

607 The project described was supported by Award Numbers F30CA35792 from the
608 National Cancer Institute (to NDN), C17199/A18246 from the Cancer Research Wales
609 and Cancer Research UK (to DMB), RP129976 from the Cancer Prevention Research
610 Institute of Texas (to AAB), W81XWH-10-1-0389 from the Department of Defense
611 Congressionally Directed Medical Research Program Bone Marrow Failure Research
612 Program (to AAB), American Society of Hematology Bridge Award (to AAB) and
613 R01HL131744 from the National Heart, Lung, and Blood Institute (to AAB). The content
614 is solely the responsibility of the authors and does not necessarily represent the official
615 views of the National Cancer Institute, the National Heart, Lung, and Blood Institute, the
616 National Institutes of Health, the Cancer Prevention Research Institute of Texas or the
617 Department of Defense Congressionally Directed Medical Research Program.

618 We would like to thank Dr. Titia De Lange (Rockefeller University) for the anti-TIN2
619 antibody and the myc-TRF1, myc-TRF2, myc-TRF2-F120A, and pSP73Sty11 vectors.
620 We are grateful to Dr. Kenneth Scott and Turgut Dogruluk (Baylor College of Medicine)
621 for the pLenti6.3 vectors, Dr. Albert Ribes-Zamora (St. Thomas University) for
622 generation of several of the TIN2 mutations, Dr. Susan Smith (NYU) for the TPP1
623 vector, Dr. Ming Lei (University of Michigan) for the pET28SUMO vector, and Lucy Gao
624 (Baylor College of Medicine) for her technical assistance.

625 NDN and AAB conceived the study and designed the experiments. NDN performed all
626 experiments except STELA and ChIP and analyzed data. LMD and CLW analyzed the
627 CRISPR/Cas9 modified cell lines. LE performed the STELA experiments, which were
628 supervised by DMB. ATS performed the ChIP experiments. I.M. performed the
629 evolutionary trace analysis. AB assessed the efficiency of the guide RNAs. NDN and
630 AAB wrote the paper with essential assistance from LMD. AAB supervised the research.

631 **REFERENCES**

632 1. **Doksani Y, Wu JY, de Lange T, Zhuang X.** 2013. Super-resolution
633 fluorescence imaging of telomeres reveals TRF2-dependent T-loop formation.
634 Cell **155:**345-356. 4062873
635 2. **Ribes-Zamora A, Indiviglio SM, Mihalek I, Williams CL, Bertuch AA.** 2013.
636 TRF2 interaction with Ku heterotetramerization interface gives insight into c-
637 NHEJ prevention at human telomeres. Cell Rep **5:**194-206. 3984498
638 3. **Okamoto K, Bartocci C, Ouzounov I, Diedrich JK, Yates JR, 3rd, Denchi EL.**
639 2013. A two-step mechanism for TRF2-mediated chromosome-end protection.
640 Nature **494:**502-505.
641 4. **Xin H, Liu D, Wan M, Safari A, Kim H, Sun W, O'Connor MS, Songyang Z.**
642 2007. TPP1 is a homologue of ciliate TEBP-beta and interacts with POT1 to
643 recruit telomerase. Nature **445:**559-562.
644 5. **Wang F, Podell ER, Zaug AJ, Yang Y, Baciu P, Cech TR, Lei M.** 2007. The
645 POT1-TPP1 telomere complex is a telomerase processivity factor. Nature
646 **445:**506-510.

647 6. **Griffith JD, Comeau L, Rosenfield S, Stansel RM, Bianchi A, Moss H, de**
648 **Lange T.** 1999. Mammalian telomeres end in a large duplex loop. Cell **97:**503-
649 514.
650 7. **Ye JZ, Donigian JR, van Overbeek M, Loayza D, Luo Y, Krutchinsky AN,**
651 **Chait BT, de Lange T.** 2004. TIN2 binds TRF1 and TRF2 simultaneously and
652 stabilizes the TRF2 complex on telomeres. J Biol Chem **279:**47264-47271.
653 8. **Canudas S, Smith S.** 2009. Differential regulation of telomere and centromere
654 cohesion by the Scc3 homologues SA1 and SA2, respectively, in human cells. J
655 Cell Biol **187:**165-173. 2768842
656 9. **Chen Y, Yang Y, van Overbeek M, Donigian JR, Baciu P, de Lange T, Lei M.**
657 2008. A shared docking motif in TRF1 and TRF2 used for differential recruitment
658 of telomeric proteins. Science **319:**1092-1096.
659 10. **Kaminker PG, Kim SH, Desprez PY, Campisi J.** 2009. A novel form of the
660 telomere-associated protein TIN2 localizes to the nuclear matrix. Cell Cycle
661 **8:**931-939.
662 11. **Hu C, Rai R, Huang C, Broton C, Long J, Xu Y, Xue J, Lei M, Chang S, Chen**
663 **Y.** 2017. Structural and functional analyses of the mammalian TIN2-TPP1-TRF2
664 telomeric complex. Cell Res **27:**1485-1502.
665 12. **Ye JZ, de Lange T.** 2004. TIN2 is a tankyrase 1 PARP modulator in the TRF1
666 telomere length control complex. Nat Genet **36:**618-623.
667 13. **Abreu E, Aritonovska E, Reichenbach P, Cristofari G, Culp B, Terns RM,**
668 **Lingner J, Terns MP.** 2010. TIN2-tethered TPP1 recruits human telomerase to
669 telomeres in vivo. Mol Cell Biol **30:**2971-2982. 2876666

670 14. **Savage SA, Giri N, Baerlocher GM, Orr N, Lansdorp PM, Alter BP.** 2008.
671 TINF2, a component of the shelterin telomere protection complex, is mutated in
672 dyskeratosis congenita. Am J Hum Genet **82:**501-509.
673 15. **Walne AJ, Vulliamy T, Beswick R, Kirwan M, Dokal I.** 2008. TINF2 mutations
674 result in very short telomeres: analysis of a large cohort of patients with
675 dyskeratosis congenita and related bone marrow failure syndromes. Blood
676 **112:**3594-3600.
677 16. **Nelson ND, Bertuch AA.** 2012. Dyskeratosis congenita as a disorder of
678 telomere maintenance. Mutat. Res. **730:**43-51. 3208805
679 17. **Vulliamy T, Marrone A, Goldman F, Dearlove A, Bessler M, Mason PJ, Dokal**
680 **I.** 2001. The RNA component of telomerase is mutated in autosomal dominant
681 dyskeratosis congenita. Nature **413:**432-435.
682 18. **Armanios M, Chen JL, Chang YP, Brodsky RA, Hawkins A, Griffin CA,**
683 **Eshleman JR, Cohen AR, Chakravarti A, Hamosh A, Greider CW.** 2005.
684 Haploinsufficiency of telomerase reverse transcriptase leads to anticipation in
685 autosomal dominant dyskeratosis congenita. Proc Natl Acad Sci U S A
686 **102:**15960-15964.
687 19. **Kim SH, Kaminker P, Campisi J.** 1999. TIN2, a new regulator of telomere
688 length in human cells. Nat Genet **23:**405-412.
689 20. **Kim SH, Beausejour C, Davalos AR, Kaminker P, Heo SJ, Campisi J.** 2004.
690 TIN2 mediates functions of TRF2 at human telomeres. J Biol Chem **279:**43799-
691 43804.

692 21. **Ye JZ, Hockemeyer D, Krutchinsky AN, Loayza D, Hooper SM, Chait BT, de**
693 **Lange T.** 2004. POT1-interacting protein PIP1: a telomere length regulator that
694 recruits POT1 to the TIN2/TRF1 complex. Genes Dev **18:**1649-1654. 478187
695 22. **Sasa GS, Ribes-Zamora A, Nelson ND, Bertuch AA.** 2012. Three novel
696 truncating TINF2 mutations causing severe dyskeratosis congenita in early
697 childhood. Clin Genet **81:**470-478. 3844870
698 23. **Xin ZT, Ly H.** 2012. Characterization of interactions between naturally mutated
699 forms of the TIN2 protein and its known protein partners of the shelterin complex.
700 Clin Genet **81:**301-302.
701 24. **Canudas S, Houghtaling BR, Bhanot M, Sasa G, Savage SA, Bertuch AA,**
702 **Smith S.** 2011. A role for heterochromatin protein 1γ at human telomeres. Genes
703 Dev **25:**1807-1819. 3175717
704 25. **Yang D, He Q, Kim H, Ma W, Songyang Z.** 2011. TIN2 protein dyskeratosis
705 congenita missense mutants are defective in association with telomerase. J Biol
706 Chem **286:**23022-23030. 3123070
707 26. **Frescas D, de Lange T.** 2014. A TIN2 dyskeratosis congenita mutation causes
708 telomerase-independent telomere shortening in mice. Genes Dev **28:**153-166.
709 3909789
710 27. **Mihalek I, Res I, Lichtarge O.** 2004. A family of evolution-entropy hybrid
711 methods for ranking protein residues by importance. J Mol Biol **336:**1265-1282.
712 28. **Flicek P, Amode MR, Barrell D, Beal K, Billis K, Brent S, Carvalho-Silva D,**
713 **Clapham P, Coates G, Fitzgerald S, Gil L, Giron CG, Gordon L, Hourlier T,**
714 **Hunt S, Johnson N, Juettemann T, Kahari AK, Keenan S, Kulesha E, Martin**

715 **FJ, Maurel T, McLaren WM, Murphy DN, Nag R, Overduin B, Pignatelli M,**
716 **Pritchard B, Pritchard E, Riat HS, Ruffier M, Sheppard D, Taylor K,**
717 **Thormann A, Trevanion SJ, Vullo A, Wilder SP, Wilson M, Zadissa A, Aken**
718 **BL, Birney E, Cunningham F, Harrow J, Herrero J, Hubbard TJ, Kinsella R,**
719 **Muffato M, Parker A, Spudich G, Yates A, Zerbino DR, Searle SM.** 2014.
720 Ensembl 2014. Nucleic Acids Res **42:**D749-755.
721 29. **Pruitt KD, Tatusova T, Maglott DR.** 2007. NCBI reference sequences (RefSeq):
722 a curated non-redundant sequence database of genomes, transcripts and
723 proteins. Nucleic Acids Res **35:**D61-65. 1716718
724 30. **Blom N, Sicheritz-Ponten T, Gupta R, Gammeltoft S, Brunak S.** 2004.
725 Prediction of post-translational glycosylation and phosphorylation of proteins from
726 the amino acid sequence. Proteomics **4:**1633-1649.
727 31. **Blom N, Gammeltoft S, Brunak S.** 1999. Sequence and structure-based
728 prediction of eukaryotic protein phosphorylation sites. J Mol Biol **294:**1351-1362.
729 32. **Xue Y, Ren J, Gao X, Jin C, Wen L, Yao X.** 2008. GPS 2.0, a tool to predict
730 kinase-specific phosphorylation sites in hierarchy. Mol Cell Proteomics **7:**1598-
731 1608. PMC2528073
732 33. **Liu D.** 2011. Analysis of Average Telomere Length in Cultured Human Cells, p.
733 13-20. *In* Songyang Z (ed.), Telomeres and Telomerase, Second ed, vol. 735.
734 Humana Press, New York.
735 34. **van Steensel B, de Lange T.** 1997. Control of telomere length by the human
736 telomeric protein TRF1. Nature **385:**740-743.

737 35. **Capper R, Britt-Compton B, Tankimanova M, Rowson J, Letsolo B, Man S,**
738 **Haughton M, Baird DM.** 2007. The nature of telomere fusion and a definition of
739 the critical telomere length in human cells. Genes Dev **21:**2495-2508. 1993879
740 36. **Hsu PD, Scott DA, Weinstein JA, Ran FA, Konermann S, Agarwala V, Li Y,**
741 **Fine EJ, Wu X, Shalem O, Cradick TJ, Marraffini LA, Bao G, Zhang F.** 2013.
742 DNA targeting specificity of RNA-guided Cas9 nucleases. Nat Biotechnol **31:**827-
743 832. 3969858
744 37. **Kim SH, Davalos AR, Heo SJ, Rodier F, Zou Y, Beausejour C, Kaminker P,**
745 **Yannone SM, Campisi J.** 2008. Telomere dysfunction and cell survival: roles for
746 distinct TIN2-containing complexes. J Cell Biol **181:**447-460.
747 38. **Dignam JD, Lebovitz RM, Roeder RG.** 1983. Accurate transcription initiation by
748 RNA polymerase II in a soluble extract from isolated mammalian nuclei. Nucleic
749 Acids Res **11:**1475-1489. 325809
750 39. **Pinna LA.** 1990. Casein kinase 2: an 'eminence grise' in cellular regulation?
751 Biochim Biophys Acta **1054:**267-284.
752 40. **Allende JE, Allende CC.** 1995. Protein kinases. 4. Protein kinase CK2: an
753 enzyme with multiple substrates and a puzzling regulation. FASEB J **9:**313-323.
754 41. **Phanstiel DH, Brumbaugh J, Wenger CD, Tian S, Probasco MD, Bailey DJ,**
755 **Swaney DL, Tervo MA, Bolin JM, Ruotti V, Stewart R, Thomson JA, Coon**
756 **JJ.** 2011. Proteomic and phosphoproteomic comparison of human ES and iPS
757 cells. Nat Methods **8:**821-827. 3432645

758 42. **Zanivan S, Gnad F, Wickstrom SA, Geiger T, Macek B, Cox J, Fassler R,**
759 **Mann M.** 2008. Solid tumor proteome and phosphoproteome analysis by high
760 resolution mass spectrometry. J Proteome Res **7:**5314-5326.
761 43. **Huttlin EL, Jedrychowski MP, Elias JE, Goswami T, Rad R, Beausoleil SA,**
762 **Villen J, Haas W, Sowa ME, Gygi SP.** 2010. A tissue-specific atlas of mouse
763 protein phosphorylation and expression. Cell **143:**1174-1189. 3035969
764 44. **Yu Y, Yoon SO, Poulogiannis G, Yang Q, Ma XM, Villen J, Kubica N,**
765 **Hoffman GR, Cantley LC, Gygi SP, Blenis J.** 2011. Phosphoproteomic analysis
766 identifies Grb10 as an mTORC1 substrate that negatively regulates insulin
767 signaling. Science **332:**1322-1326. 3195509
768 45. **Kim MK, Kang MR, Nam HW, Bae YS, Kim YS, Chung IK.** 2008. Regulation of
769 telomeric repeat binding factor 1 binding to telomeres by casein kinase 2-
770 mediated phosphorylation. J Biol Chem **283:**14144-14152.
771 46. **Kinoshita E, Kinoshita-Kikuta E, Takiyama K, Koike T.** 2006. Phosphate-
772 binding tag, a new tool to visualize phosphorylated proteins. Mol Cell Proteomics
773 **5:**749-757.
774 47. **Yang S, Counter CM.** 2013. Cell Cycle Regulated Phosphorylation of the
775 Telomere-Associated Protein TIN2. PLoS One **8:**e71697. 3745427
776 48. **Wang G, Unger G, Ahmad KA, Slaton JW, Ahmed K.** 2005. Downregulation of
777 CK2 induces apoptosis in cancer cells--a potential approach to cancer therapy.
778 Mol Cell Biochem **274:**77-84.
779 49. **Sarno S, Reddy H, Meggio F, Ruzzene M, Davies SP, Donella-Deana A,**
780 **Shugar D, Pinna LA.** 2001. Selectivity of 4,5,6,7-tetrabromobenzotriazole, an

781 ATP site-directed inhibitor of protein kinase CK2 ('casein kinase-2'). FEBS Lett
782 **496:**44-48.
783 50. **Remy I, Montmarquette A, Michnick SW.** 2004. PKB/Akt modulates TGF-beta
784 signalling through a direct interaction with Smad3. Nat. Cell Biol. **6:**358-365.
785 51. **Kim H, Lee OH, Xin H, Chen LY, Qin J, Chae HK, Lin SY, Safari A, Liu D,**
786 **Songyang Z.** 2009. TRF2 functions as a protein hub and regulates telomere
787 maintenance by recognizing specific peptide motifs. Nat Struct Mol Biol **16:**372-
788 379.
789 52. **Liu D, O'Connor MS, Qin J, Songyang Z.** 2004. Telosome, a mammalian
790 telomere-associated complex formed by multiple telomeric proteins. J Biol Chem
791 **279:**51338-51342.
792 53. **Lim CJ, Zaug AJ, Kim HJ, Cech TR.** 2017. Reconstitution of human shelterin
793 complexes reveals unexpected stoichiometry and dual pathways to enhance
794 telomerase processivity. Nat Commun **8:**1075. PMC5651854
795 54. **Cho SW, Kim S, Kim JM, Kim JS.** 2013. Targeted genome engineering in
796 human cells with the Cas9 RNA-guided endonuclease. Nat Biotechnol **31:**230-
797 232.
798 55. **Kim H, Li F, He Q, Deng T, Xu J, Jin F, Coarfa C, Putluri N, Liu D, Songyang**
799 **Z.** 2017. Systematic analysis of human telomeric dysfunction using inducible
800 telosome/shelterin CRISPR/Cas9 knockout cells. Cell Discov **3:**17034.
801 PMC5613224
802 56. **Takai KK, Hooper S, Blackwood S, Gandhi R, de Lange T.** 2010. In vivo
803 stoichiometry of shelterin components. J Biol Chem **285:**1457-1467. 2801271

804 57. **Wan B, Yin J, Horvath K, Sarkar J, Chen Y, Wu J, Wan K, Lu J, Gu P, Yu EY,
805 Lue NF, Chang S, Liu Y, Lei M.** 2013. SLX4 assembles a telomere maintenance
806 toolkit by bridging multiple endonucleases with telomeres. Cell Rep. **4:**861-869.
807 4334113
808 58. **Lam YC, Akhter S, Gu P, Ye J, Poulet A, Giraud-Panis MJ, Bailey SM, Gilson
809 E, Legerski RJ, Chang S.** 2010. SNMIB/Apollo protects leading-strand
810 telomeres against NHEJ-mediated repair. EMBO J. **29:**2230-2241. 2905253

811 **Competing Financial Interests**

812 The authors declare no competing financial interests.

813 **FIGURE LEGENDS**

814 **Figure 1.** TIN2L phosphorylation is dependent upon an intact CK2 consensus site. (A)
815 Evolutionary trace analysis and summary of known interaction regions in TIN2. The
816 residues comprising the putative CK2 phosphorylation sites are displayed. The protein
817 interaction domains, the region where all DC causing mutations cluster (DC), the
818 position of R282 (*), and the putative TBM, all of which are present in both the TIN2L
819 and TIN2S isoforms, and the C-terminal domain unique to TIN2L (TIN2L CTD) are
820 indicated. (B) Characterization of TIN2S and TIN2L phosphorylation. Flag tagged TIN2S
821 or TIN2L was analyzed by SDS-PAGE in the presence of Phos-tag reagent.
822 Phosphorylated TIN2L ($TIN2L^P$) is visible as a supershift compared to the λ
823 phosphatase-treated TIN2L. (C) Characterization of TIN2L phosphorylation at S396 as
824 in (B). (D) Recombinant CK2 (NEB) analyzed by SDS-PAGE and silver staining. M,
825 protein molecular weight marker; 1, CK2 (E) *In vitro* phosphorylation of TIN2L by CK2.
826 Recombinant TIN2L purified from *E. coli* was incubated with CK2 and [γ-32P]-ATP in the

827 absence or presence of a CK2 inhibitor (TBB). (F) *In vitro* phosphorylation of partially
828 purified TIN2L and TIN2L-S396A by CK2. Flag tagged TIN2L or TIN2L-S396A from
829 transiently transfected 293T cells was dephosphorylated by incubation with λ
830 phosphatase, purified via immunoprecipitation, and incubated with CK2.
831 Phosphorylation status was assessed by SDS-PAGE in the presence of the Phos-tag
832 reagent and compared to non-λ phosphatase treated controls.

833 **Figure 2.** S396 phosphorylation and R282 cooperate to promote TIN2L binding to
834 TRF2. (A) Representative co-IP of TRF2 with co-transfected wild type TIN2S/L or
835 TIN2S/L-R282H. (B) Representative co-IP of TRF2 with co-transfected wild type
836 TIN2S/L, phosphomimetic TIN2L (S396E) or phosphodead TIN2L (S396A). (C)
837 Representative co-IP of TRF2 with co-transfected wild type TIN2S/L, TIN2L-R282H,
838 TIN2L-S396A, or double mutant TIN2L-R282H+S396A. (D) Quantification of (A), (B),
839 and (C). For quantification, the amount of TRF2 co-immunoprecipitated was divided by
840 the amount of TIN2 immunoprecipitated in order to account for any differences in TIN2
841 expression/pull down. For each experiment, the value was then normalized to that of
842 TIN2S. Error bars represent the standard deviation (SD) of several separate co-IP
843 experiments. * $p<0.008$.

844 **Figure 3**. The protein complementation assay confirms the effects of the R282H
845 mutation and a phosphorylation site mutation on TIN2L interaction with TRF2. (A)
846 Quantification of fluorescence from co-expression of V1-TRF2 with TIN2L-V2, TIN2L-
847 D391K+D395K-V2 or TIN2L-R282H-V2. Error bars represent the SD of three separate

848 transfections each measured in triplicate. *p<0.001. (B) Western blot exhibiting
849 expression of the proteins assayed in (A).

850 **Figure 4.** Interaction of TIN2L with TRF2 requires TRF2-F120. (A) Representative co-IP
851 of TIN2S or TIN2L co-transfected with TRF2 or TRF2-F120A. (B) Quantification of (A).
852 Error bars represent the SD of several separate co-IP experiments. For quantification,
853 the amount of TRF2 co-immunoprecipitated was divided by the amount of TIN2
854 immunoprecipitated in order to account for any differences in TIN2 expression/pull
855 down. For each experiment, the value was then normalized to that of TIN2S. * p<0.05.

856 **Figure 5.** TIN2L interacts less robustly with TRF1 than TIN2S, but both isoforms
857 interact at similar levels with TPP1. (A) Representative co-IP of TRF1 co-transfected
858 with wild type TIN2S/L, TIN2S/L-R282H, and TIN2L-S396A. (B) Quantification of (A).
859 For quantification, the amount of TRF1 co-immunoprecipitated was divided by the
860 amount of TIN2 immunoprecipitated in order to account for any differences in TIN2
861 expression/pull down. For each experiment, the value was then normalized to that of
862 TIN2S. Error bars represent the SD of several separate co-IP experiments. * p <0.02
863 (C) Representative co-IP of TPP1 co-transfected with wild type TIN2S/L, TIN2S/L-
864 R282H, and TIN2L-S396A. (D) Quantification of (C). For quantification, the amount of
865 TPP1 co-immunoprecipitated was divided by the amount of TIN2 immunoprecipitated in
866 order to account for any differences in TIN2 expression/pull down. For each experiment,
867 the value was then normalized to that of TIN2S. Error bars represent the SD of several
868 separate co-IP experiments.

869 **Figure 6.** Endogenous TIN2L co-fractionates with other shelterin components in HeLa
870 cell nuclear extract. (A) Western blot analysis of shelterin components from size based
871 fractionation of HeLa cell nuclear lysate. HeLa cell nuclear extracts were subjected to
872 gel filtration, and 0.5 mL fractions were taken beginning at 30 mL elution volume. 50 μL
873 aliquots were taken from the indicated fractions and analyzed for the presence of TIN2,
874 TRF1, TRF2, and POT1 by immunoblotting. The molecular size indicated was
875 determined using a molecular weight standard. (B) Quantification of (A). Values were
876 normalized to the fraction with the highest amount of each respective protein.

877 **Figure 7.** Loss of TIN2L phosphorylation inhibits progressive telomere elongation in
878 telomerase positive HT1080 cells. (A) Representative telomere Southern blot analysis
879 of telomere length in kilobasepairs (kb) over time in HT1080 cells overexpressing
880 TIN2S, TIN2S-R282H, TIN2L, TIN2L-S396A, or TIN2L-S396E. HT1080 cells
881 overexpressing the indicated TIN2 proteins were collected at various times following
882 induction with lentivirus and blastocidin selection and analyzed by the terminal
883 restriction fragment assay. (B) Quantification of (A) using densitometry analysis. Error
884 bars indicate the SD of two separate terminal restriction fragment assays. (C) Western
885 blot showing TIN2 expression levels in each cell line. Total cell protein lysates were
886 prepared using 2X Laemmli buffer.

887 **Figure 8.** Telomere lengths of TIN2L mutant HT1080 cell lines are indistinguishable
888 from TIN2L wildtype lines. (A) XpYp STELA analysis of DNA isolated at the indicated
889 numbers of days from the point of clonal line derivation. Mean lengths, SD, and
890 standard error (SD) in kb are indicated. +veC, 293 cell line. (B) Individual telomere
891 lengths in the designated lines at the designated days.

892 **Figure 9**. The telomere association of TRF1 and TRF2 is unaffected by loss of TIN2L
893 function. Endogenous TRF1 and TRF2 were immunoprecipitated from lysates prepared
894 from formaldehyde crosslinked cells. Association with telomeric DNA was assessed by
895 (A) Southern blotting. IgG and Alu probes were included as controls for nonspecific
896 association. (B) Average percent telomeric DNA in IP relative to input, +/- 1 SD (n=3).

Nelson Figure 1

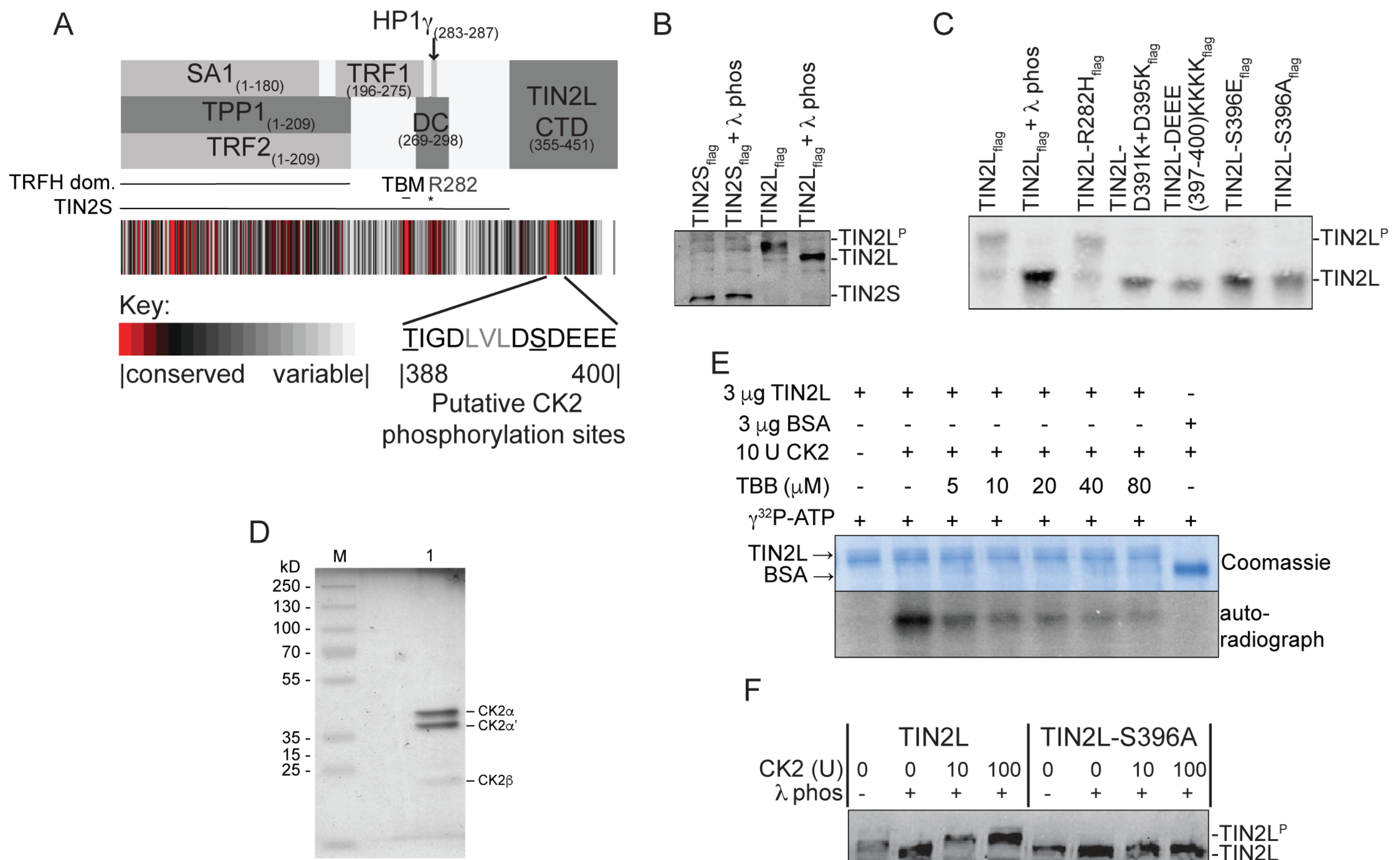

Figure 1. TIN2L phosphorylation is dependent upon an intact CK2 consensus site. (A) Evolutionary trace analysis and summary of known interaction regions in TIN2. The residues comprising the putative CK2 phosphorylation sites are displayed. The protein interaction domains, the region where all DC causing mutations cluster (DC), the position of R282 (*), and the putative TBM, all of which are present in both the TIN2L and TIN2S isoforms, and the C-terminal domain unique to TIN2L (TIN2L CTD) are indicated. (B) Characterization of TIN2S and TIN2L phosphorylation. Flag tagged TIN2S or TIN2L was analyzed by SDS-PAGE in the presence of Phos-tag reagent. Phosphorylated TIN2L ($TIN2L^P$) is visible as a supershift compared to the λ phosphatase-treated TIN2L. (C) Characterization of TIN2L phosphorylation at S396 as in (B). (D) Recombinant CK2 (NEB) analyzed by SDS-PAGE and silver staining. M, protein molecular weight marker; 1, CK2 (E) In vitro phosphorylation of TIN2L by CK2. Recombinant TIN2L purified from E. coli was incubated with CK2 and [γ-32P]-ATP in the absence or presence of a CK2 inhibitor (TBB). (F) In vitro phosphorylation of partially purified TIN2L and TIN2L-S396A by CK2. Flag tagged TIN2L or TIN2L-S396A from transiently transfected 293T cells was dephosphorylated by incubation with λ phosphatase, purified via immunoprecipitation, and incubated with CK2. Phosphorylation status was assessed by SDS-PAGE in the presence of the Phos-tag reagent and compared to non-λ phosphatase treated controls.

Nelson Figure 2

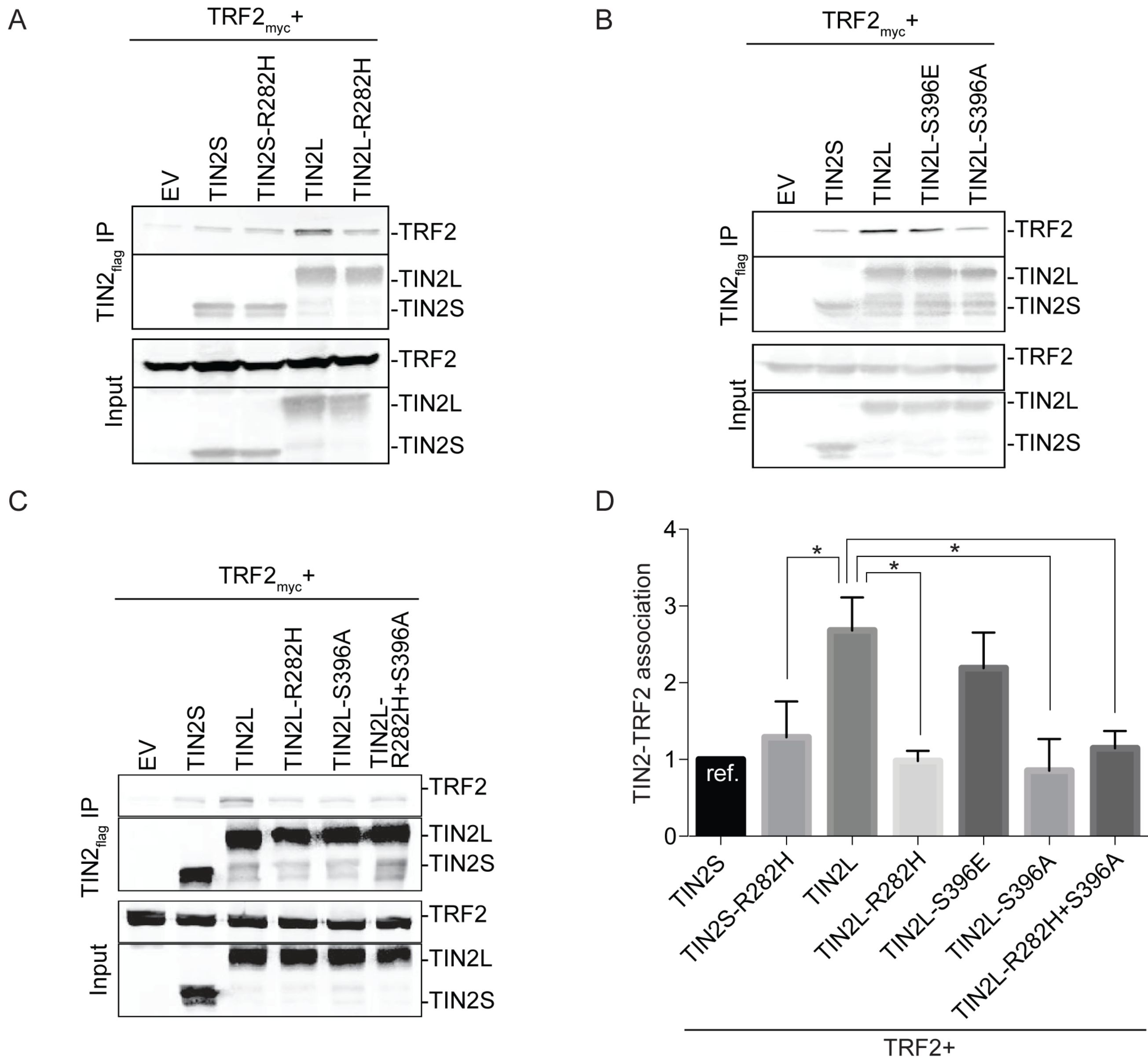

Figure 2. S396 phosphorylation and R282 cooperate to promote TIN2L binding to TRF2. (A) Representative co-IP of TRF2 with co-transfected wild type TIN2S/L or TIN2S/L-R282H. (B) Representative co-IP of TRF2 with co-transfected wild type TIN2S/L, phosphomimetic TIN2L (S396E) or phosphodead TIN2L (S396A). (C) Representative co-IP of TRF2 with co-transfected wild type TIN2S/L, TIN2L-R282H, TIN2L-S396A, or double mutant TIN2L-R282H+S396A. (D) Quantification of (A), (B), and (C). For quantification, the amount of TRF2 co-immunoprecipitated was divided by the amount of TIN2 immunoprecipitated in order to account for any differences in TIN2 expression/pull down. For each experiment, the value was then normalized to that of TIN2S. Error bars represent the SD of several separate co-IP experiments. * $p<0.008$.

Nelson Figure 3

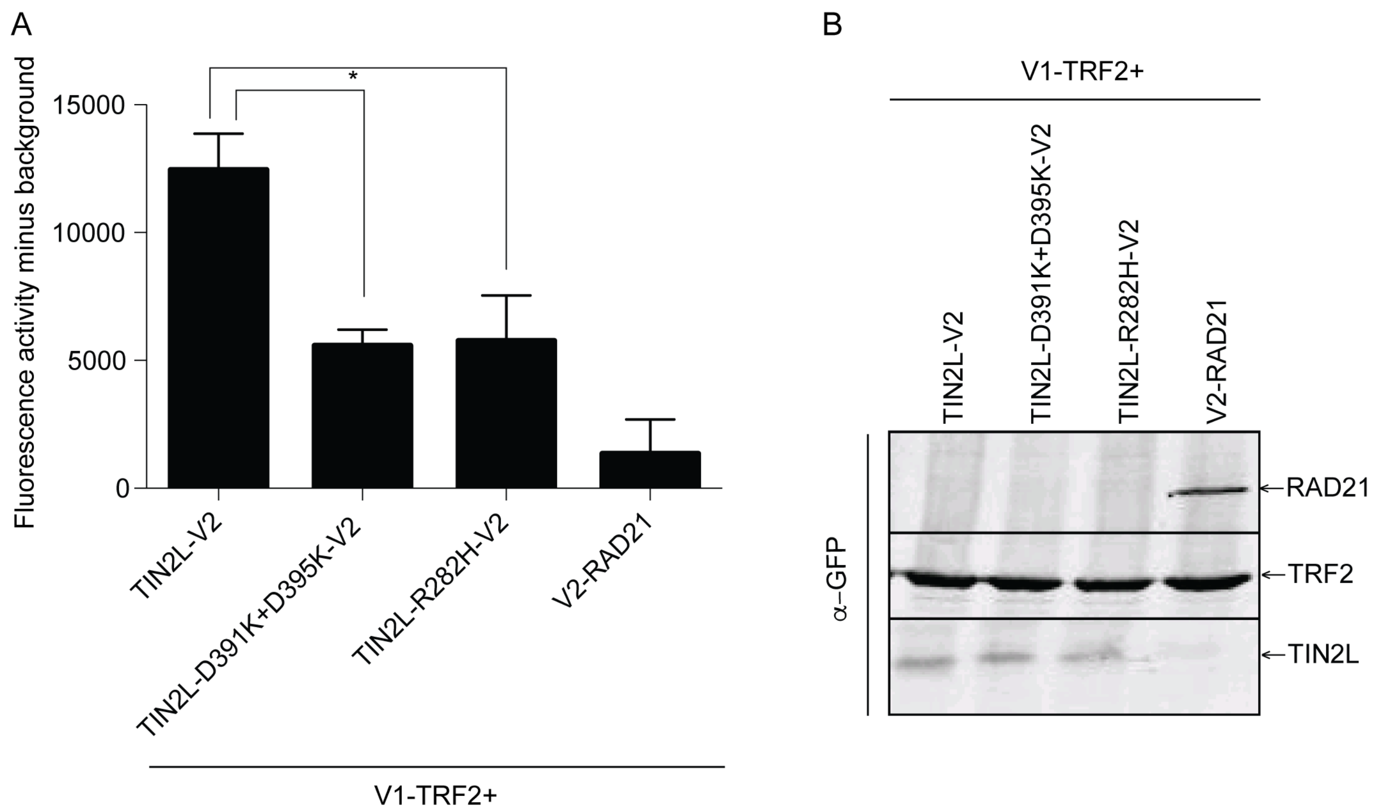

Figure 3. The protein complementation assay confirms the effects of the R282H mutation and a phosphorylation site mutation on TIN2L interaction with TRF2. (A) Quantification of fluorescence from co-expression of V1-TRF2 with TIN2L-V2, TIN2L-D391K+D395K-V2 or TIN2L-R282H-V2. Error bars represent the SD of three separate transfections each measured in triplicate. *p<0.001. (B) Western blot exhibiting expression of the proteins assayed in (A).

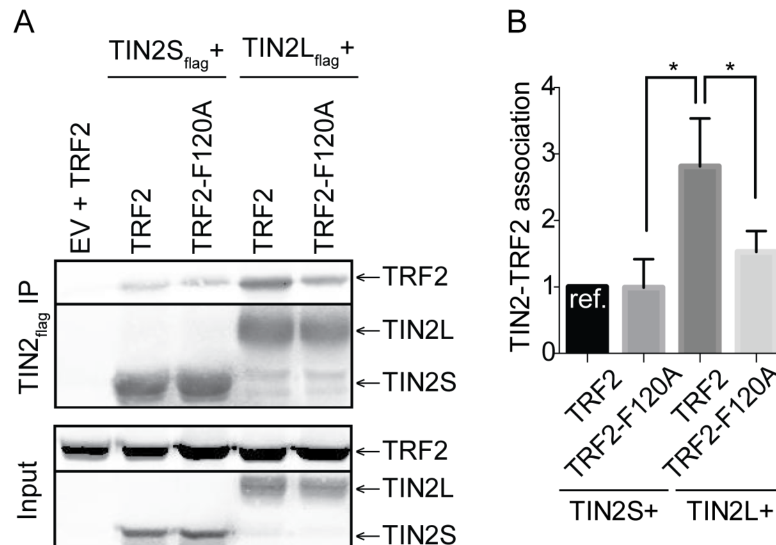

Figure 4. Interaction of TIN2L with TRF2 requires TRF2-F120. (A) Representative co-IP of TIN2S or TIN2L co-transfected with TRF2 or TRF2-F120A. (B) Quantification of (A). Error bars represent the SD of several separate co-IP experiments. For quantification, the amount of TRF2 co-immunoprecipitated was divided by the amount of TIN2 immunoprecipitated in order to account for any differences in TIN2 expression/pull down. For each experiment, the value was then normalized to that of TIN2S. * $p<0.05$.

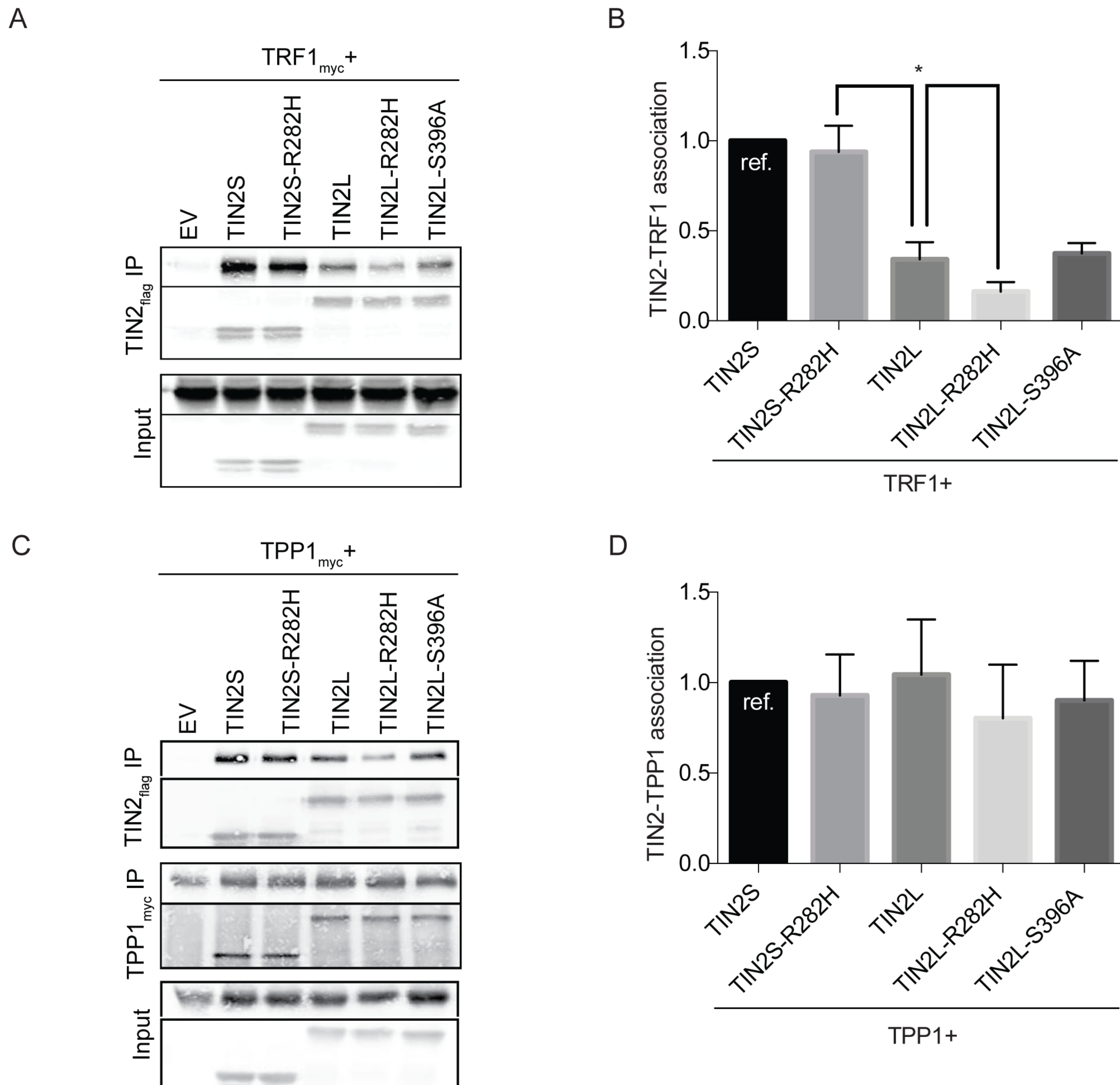

Figure 5. TIN2L interacts less robustly with TRF1 than TIN2S, but both isoforms interact at similar levels with TPP1. (A) Representative co-IP of TRF1 co-transfected with wild type TIN2S/L, TIN2S/L-R282H, and TIN2L-S396A. (B) Quantification of (A). For quantification, the amount of TRF1 co-immunoprecipitated was divided by the amount of TIN2 immunoprecipitated in order to account for any differences in TIN2 expression/pull down. For each experiment, the value was then normalized to that of TIN2S. Error bars represent the SD of several separate co-IP experiments. * $p < 0.02$ (C) Representative co-IP of TPP1 co-transfected with wild type TIN2S/L, TIN2S/L-R282H, and TIN2L-S396A. (D) Quantification of (C). For quantification, the amount of TPP1 co-immunoprecipitated was divided by the amount of TIN2 immunoprecipitated in order to account for any differences in TIN2 expression/pull down. For each experiment, the value was then normalized to that of TIN2S. Error bars represent the SD of several separate co-IP experiments.

Nelson Figure 6

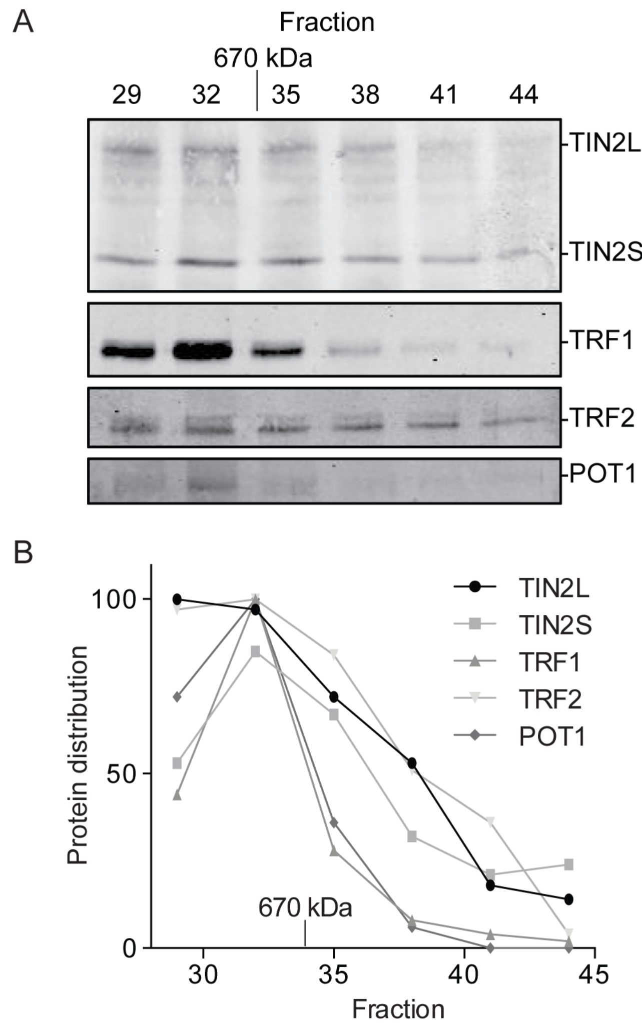

Figure 6. Endogenous TIN2L co-fractionates with other shelterin components in HeLa cell nuclear extract. (A) Western blot analysis of shelterin components from size based fractionation of HeLa cell nuclear lysate. HeLa cell nuclear extracts were subjected to gel filtration, and 0.5 mL fractions were taken beginning at 30 mL elution volume. 50 μL aliquots were taken from the indicated fractions and analyzed for the presence of TIN2, TRF1, TRF2, and POT1 by immunoblotting. The molecular size indicated was determined using a molecular weight standard. (B) Quantification of (A). Values were normalized to the fraction with the highest amount of each respective protein.

Nelson Figure 7

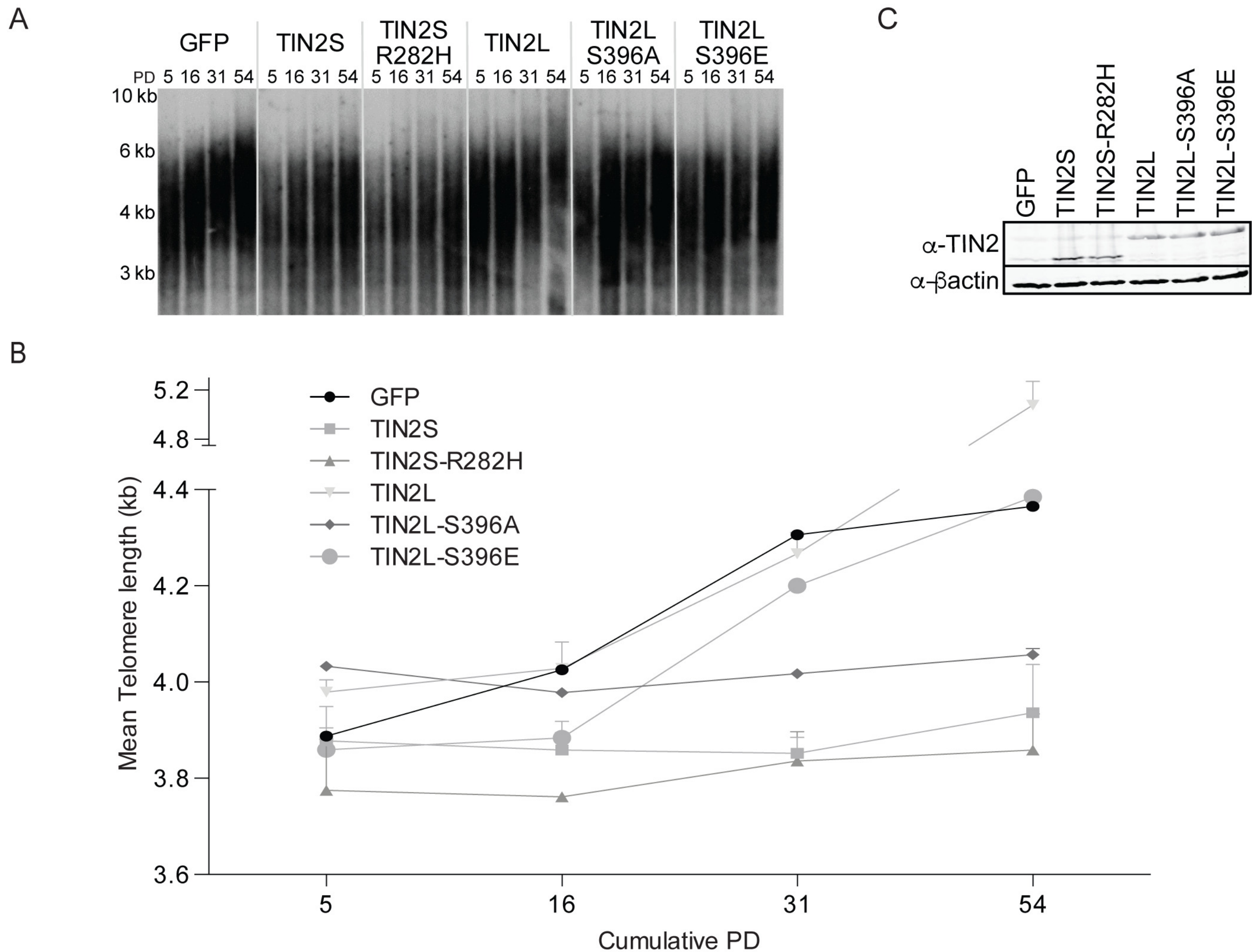

Figure 7. Loss of TIN2L phosphorylation inhibits progressive telomere elongation in telomerase positive HT1080 cells. (A) Representative telomere Southern blot analysis of telomere length in kilobasepairs (kb) over time in HT1080 cells overexpressing TIN2S, TIN2S-R282H, TIN2L, TIN2L-S396A, or TIN2L-S396E. HT1080 cells overexpressing the indicated TIN2 proteins were collected at various times following induction with lentivirus and blastocidin selection and analyzed by the terminal restriction fragment assay. (B) Quantification of (A) using densitometry analysis. Error bars indicate the SD of two separate terminal restriction fragment assays. (C) Western blot showing TIN2 expression levels in each cell line. Total cell protein lysates were prepared using 2X Laemmli buffer.

Nelson Figure 8

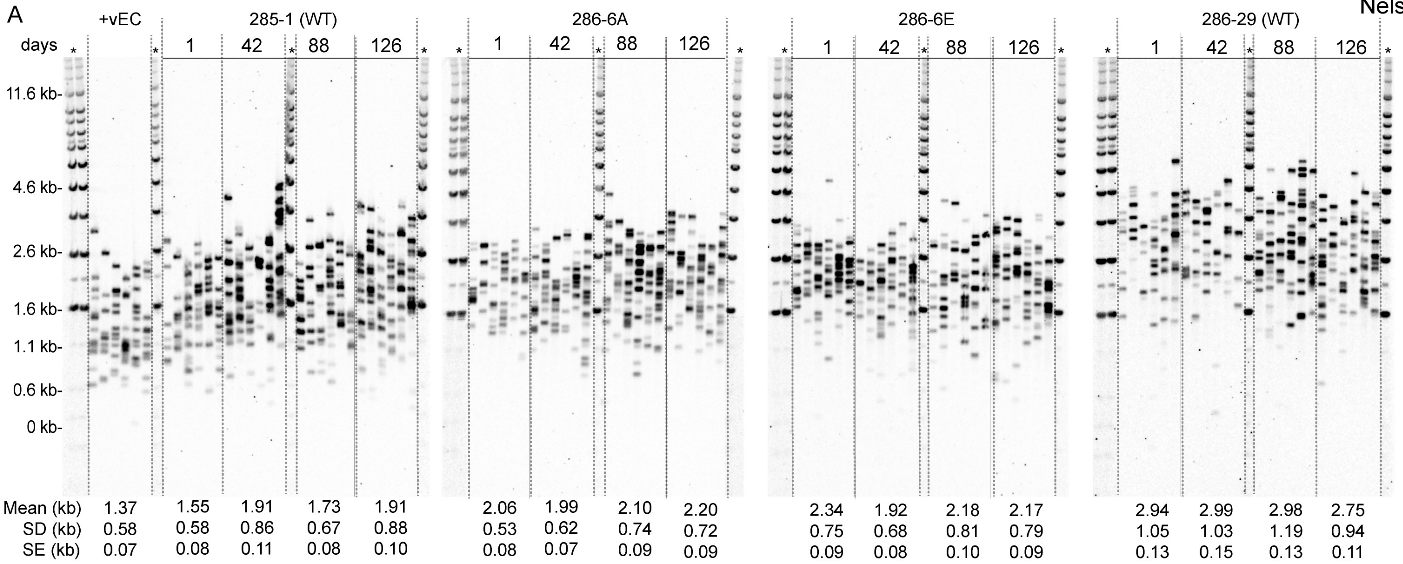

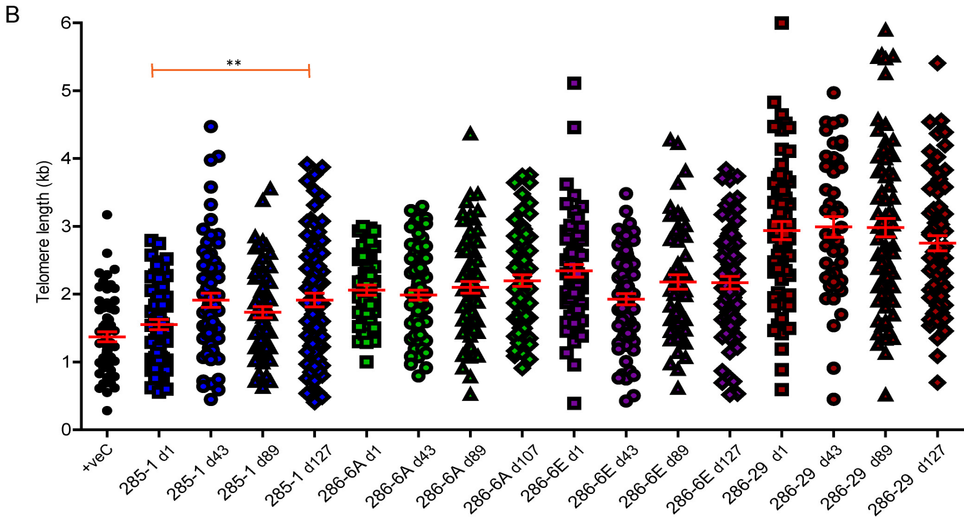

Figure 8. Telomere lengths of TIN2L mutant HT1080 cell lines are indistinguishable from TIN2L wildtype lines. (A) STELA analysis of DNA isolated at the indicated numbers of days from the point of clonal line derivation. Mean lengths, SD, and standard error (SE) in kb are indicated. +veC, 293 cell line. (B) Individual telomere lengths in the designated lines at the designated days.

Nelson Figure 9

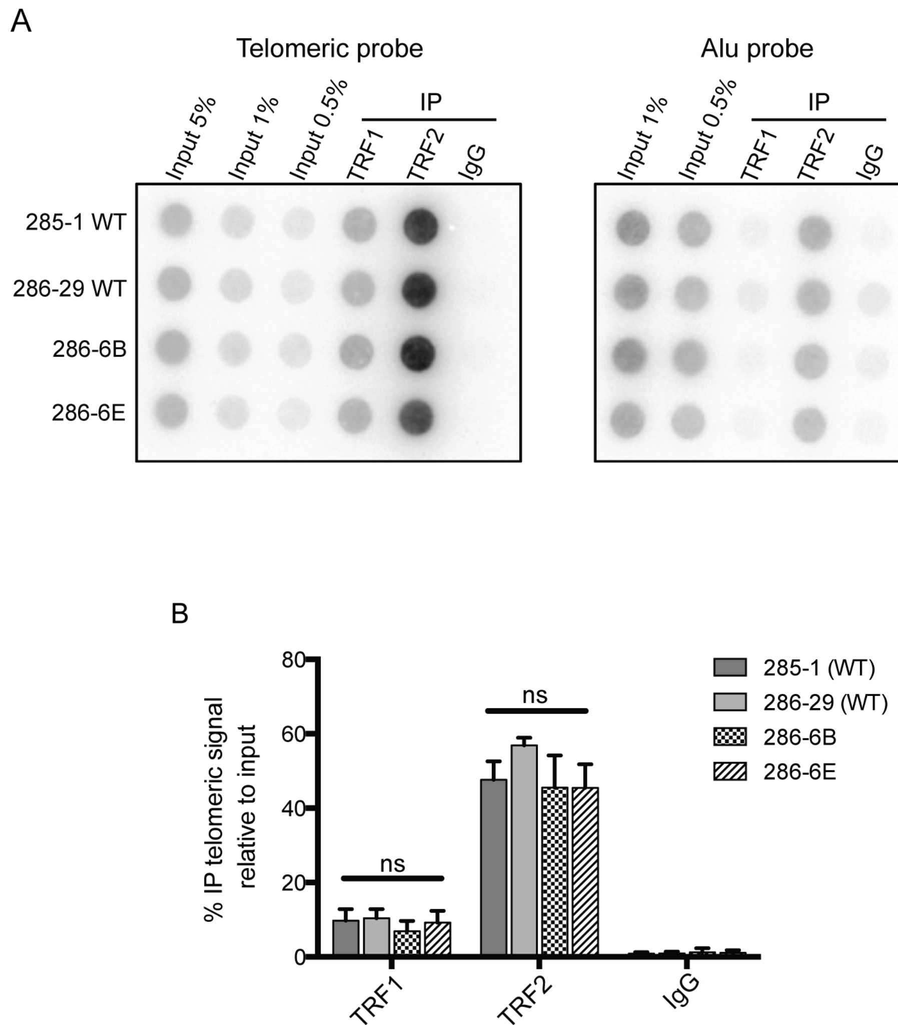

Figure 9. The telomere association of TRF1 and TRF2 is unaffected by loss of TIN2L function. Endogenous TRF1 and TRF2 were immunoprecipitated from lysates prepared from formaldehyde crosslinked cells. Association with telomeric DNA was assessed by (A) Southern blotting. IgG and Alu probes were included as controls for nonspecific association. (B) Average percent telomeric DNA in IP relative to input, +/- 1 SD (n=3).